



Chinese Pharmaceutical Association
Institute of Materia Medica, Chinese Academy of Medical Sciences

Acta Pharmaceutica Sinica B

www.elsevier.com/locate/apsb
www.sciencedirect.com



ORIGINAL ARTICLE

Novel benzothiazole derivatives target the Gac/Rsm two-component system as antibacterial synergists against *Pseudomonas aeruginosa* infections



Jun Liu^{a,c,†}, Wenfu Wu^{a,†}, Jiayi Hu^{a,†}, Siyu Zhao^a, Yiqun Chang^e,
Qiuxian Chen^a, Yujie Li^a, Jie Tang^a, Zhenmeng Zhang^a, Xiao Wu^a,
Shumeng Jiao^a, Haichuan Xiao^a, Qiang Zhang^a, Jiarui Du^a,
Jianfu Zhao^d, Kaihe Ye^a, Meiyan Huang^a, Jun Xu^a, Haibo Zhou^{a,*},
Junxia Zheng^{c,*}, Pinghua Sun^{a,b,d,*}

^aState Key Laboratory of Bioactive Molecules and Druggability Assessment, College of Pharmacy, Jinan University, Guangzhou 510632, China

^bKey Laboratory of Xinjiang Phytomedicine Resource and Utilization, Ministry of Education, School of Pharmacy, Shihezi University, Shihezi 832003, China

^cSchool of Biomedical and Pharmaceutical Sciences, Guangdong University of Technology, Guangzhou 510006, China

^dDepartment of Oncology, the First Affiliated Hospital of Jinan University Guangzhou, Guangzhou 510632, China

^eFaculty of Medicine and Health, the University of Sydney, Sydney NSW 2006, Australia

Received 21 March 2024; received in revised form 1 August 2024; accepted 1 August 2024

KEY WORDS

Pseudomonas aeruginosa;
Biofilm;
Antibiotic resistant;
Two-component system;
Antibacterial synergist

Abstract The management of antibiotic-resistant, bacterial biofilm infections in skin wounds poses an increasingly challenging clinical scenario. *Pseudomonas aeruginosa* infection is difficult to eradicate because of biofilm formation and antibiotic resistance. In this study, we identified a new benzothiazole derivative compound, **SN12** (IC₅₀ = 43.3 nmol/L), demonstrating remarkable biofilm inhibition at nanomolar concentrations *in vitro*. In further activity assays and mechanistic studies, we formulated an unconventional strategy for combating *P. aeruginosa*-derived infections by targeting the two-component (Gac/Rsm) system. Furthermore, **SN12** slowed the development of ciprofloxacin and tobramycin resistance. By

*Corresponding authors.

E-mail addresses: haibo.zhou@jnu.edu.cn (Haibo Zhou), junxiazheng@gdut.edu.cn (Junxia Zheng), pinghuasunny@163.com (Pinghua Sun).

†These authors made equal contributions to this work.

Peer review under the responsibility of Chinese Pharmaceutical Association and Institute of Materia Medica, Chinese Academy of Medical Sciences.

<https://doi.org/10.1016/j.apsb.2024.08.002>

2211-3835 © 2024 The Authors. Published by Elsevier B.V. on behalf of Chinese Pharmaceutical Association and Institute of Materia Medica, Chinese Academy of Medical Sciences. This is an open access article under the CC BY-NC-ND license (<http://creativecommons.org/licenses/by-nc-nd/4.0/>).

using murine skin wound infection models, we observed that **SN12** significantly augmented the antibacterial effects of three widely used antibiotics—tobramycin (100-fold), vancomycin (200-fold), and ciprofloxacin (1000-fold)—compared with single-dose antibiotic treatments for *P. aeruginosa* infection *in vivo*. The findings of this study suggest the potential of **SN12** as a promising antibacterial synergist, highlighting the effectiveness of targeting the two-component system in treating challenging bacterial biofilm infections in humans.

© 2024 The Authors. Published by Elsevier B.V. on behalf of Chinese Pharmaceutical Association and Institute of Materia Medica, Chinese Academy of Medical Sciences. This is an open access article under the CC BY-NC-ND license (<http://creativecommons.org/licenses/by-nc-nd/4.0/>).

1. Introduction

Bacterial persistence and the proliferation of bacterial biofilms and multidrug-resistant pathogens are rapidly increasing, partly driven by the excessive use of antibiotics in both medical and agricultural settings^{1–3}. Antibiotic resistance poses a major threat to human health, as several reports indicate that antibiotic production lines are not generating sufficient drug candidates^{4,5}. Epidemiological studies have discovered that *Pseudomonas aeruginosa* is the causative agent of over 500,000 annual deaths worldwide^{6,7}. This high mortality rate is primarily attributed to biofilms, which are implicated in more than 80% of bacterial infections⁸. Biofilm-forming bacteria produce a sticky matrix composed of polysaccharides, proteins, DNA, and other compounds, creating a robust physical barrier that hinders antibiotics and the immune system from effectively targeting the bacteria^{9–11}. The ability of biofilms to slow growth and enter a dormant state initiates the progression of chronic infections, nullifying the effectiveness of antibiotic treatments^{12,13}.

Bacteria within biofilms are 10–1000 times more resistant to antibiotics than planktonic organisms. The formation of surface-associated microbial communities enables bacteria to survive in the presence of high antibiotic concentrations, thereby contributing to treatment failure and infection recurrence^{11,14,15}. Despite extensive efforts in antibiotic development, the clinical translation of these agents has been hindered by challenges such as toxicity, definition of structure–activity relationships, and pharmacoeconomic considerations^{16–18}. Therefore, developing strategies for restoring the efficacy of antibiotics against drug-resistant biofilms has become urgent¹⁹.

An unconventional approach to combating drug-resistant biofilms involves disrupting biofilm formation and virulence expression by exploiting the nutritional vulnerabilities of bacteria, with a particular focus on targeting two-component systems (TCSs) involved in bacterial metabolism^{20,21}. TCSs operate through a signal-response coupling mechanism that enables bacteria to recognize and respond to signals in diverse environments^{22,23}. These systems comprise a membrane-embedded histidine kinase sensor (HK) and a homologous response regulator (RR). HK auto phosphorylation in response to external stimuli activates the RR through phosphoryl transfer, thereby mediating the regulation and expression of various downstream target genes^{24,25}. One notable TCSs is GacS/GacA, a HK/RR-regulated system that governs bacterial colonisation strategies, virulence expression, and biofilm formation, ultimately leading to antibiotic resistance in *P. aeruginosa*^{20,26}.

Recent research has revealed that inhibiting the Gac/Rsm system increases the susceptibility of chronic bacterial infections

to antibiotics, potentially contributing to the development of antibacterial synergists that counter antibiotic resistance^{27–29}. Although such an increase may contribute to the development of antibacterial synergists that counter antibiotic resistance, progress in this direction has been limited. In this study, we proposed an unconventional strategy for combating *P. aeruginosa*-derived infections by targeting TCSs (Fig. 1). We identified a novel chemical class of benzothiazole, **SN12** (IC₅₀ = 43.3 nmol/L), which exhibited an outstanding ability to inhibit biofilm formation at nanomolar concentrations. Our findings indicate that **SN12** functions as an inhibitor of the Gac/Rsm system, effectively reducing biofilm formation and virulence expression. We evaluated the effects of **SN12** in murine infection models and demonstrated its ability to enhance the antibacterial effects of three well-known antibiotics—tobramycin (100-fold) vancomycin (200-fold), and ciprofloxacin (1000-fold)—compared with single-dose antibiotic treatments in a mouse model infected by *P. aeruginosa*. Furthermore, **SN12** significantly reduced the development of antibiotic resistance. This is ground-breaking study to report a new benzothiazole derivative that holds promise as a potential drug for the treatment of bacterial resistance.

2. Results

2.1. Chemistry

In our previous work, we discovered that the benzothiazole scaffold has micromolar anti-biofilm activity against *P. aeruginosa* biofilms^{30,31}. In a study of two-component (Gac/Rsm) inhibition, Carlson et al. showed that the 2-aminobenzothiazole scaffold exhibits robust HK inhibitory activity and antibacterial virulence by inhibiting the phosphorylation of GacS/GacA^{20,32}. Given that the Gac/Rsm two-component system not only regulates the expression of virulence factors but also controls biofilm formation through the modulation of extracellular polysaccharide production and flagellum formation, it can be concluded that the 2-aminobenzothiazole scaffold holds promise as a novel anti-biofilm inhibitor for further development²⁶. To enhance the anti-biofilm activity of the 2-aminobenzothiazole molecular scaffold, we have undertaken the development of a series of benzothiazole derivatives. Noting the essential role of quorum sensing signaling molecules in the regulation of bacterial biofilm formation and virulence, we observed that they commonly possess long hydrophobic alkyl chains. This common characteristic is related to the hydrophobic region of target binding, prompting us to introduce a long alkyl chain into the benzothiazole scaffold and connect it with a linker¹⁰. The goal of this approach is to facilitate the

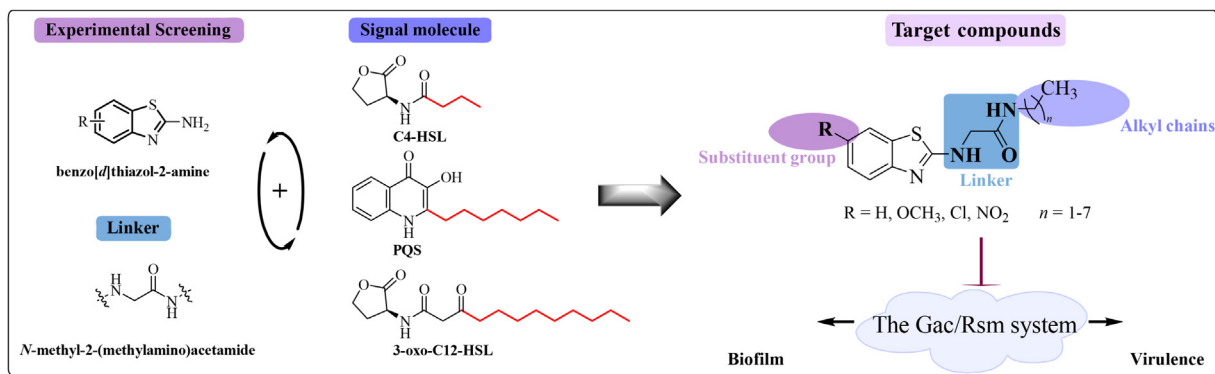


Figure 1 Structural design based on 2-aminobenzothiazole and quorum sensing signaling molecules.

development of dual potentiators that possess both anti-biofilm and anti-virulence properties (Fig. 1). The novel benzothiazole derivatives were prepared *via* four short synthetic routes in our design and synthesis experiments. Scheme 1 shows the reaction of differently substituted 2-aminobenzothiazoles with Boc anhydride to produce intermediates **1a–1d**, which were then treated with methyl bromoacetate in the presence of NaH to give intermediates **2a–2d**. Subsequently, the ester group of **2a–2d** was hydrolyzed to give intermediates **3a–3d**, followed by condensing with alkylamines of different chain lengths *via* the carboxyl group to obtain the target products **SN1–SN26**. Additionally, **SN12** was treated with Lawesson reagent to yield the thiosubstituted product **SN46**.

To investigate the significance of benzothiazole as a parent compound, we coupled the benzene and thiazole rings. As depicted in Scheme 2, alkylamines of different lengths were reacted with chloroacetyl chloride to obtain intermediates **4a–4c**, which were then subjected to nucleophilic substitution with anilines of different substituents to give the target products **SN27–SN36**. Additionally, a further portion of the intermediates were substituted with 2-aminothiazole to produce the target products **SN37–SN39**.

Furthermore, the compatibility of the linker was investigated (Scheme 3). Intermediate **5** was obtained from 2-amino-6-methoxybenzothiazole by reaction with chloroacetyl chloride. The products **SN40** and **SN41** were obtained by the reaction of hexanamine or heptanamine with **5**. On the other hand, in order to study the influence of different ring structures on anti-biofilm activity, 2-amino-6-methoxybenzothiazole was used as starting material to obtain intermediate **3b** by Boc protection and then added with an acetic acid group. Further condensation of **3b** with different amines gave the products **SN42–SN45**.

In order to investigate the influence of different substituents on the activity of benzothiazole derivatives, we have introduced electron-donating substituents onto the benzothiazole core and limited the alkyl chain length to 6. As is demonstrated in Scheme 4, benzothiazoles with electron-donating substituents were used, which undergo Boc protection, methyl bromoacetate substitution, and subsequent hydrolysis reaction to give the intermediates **3e–3h**, following a step similar to that of Scheme 1. The condensation reaction was then carried out with hexylamine, and the products **SN47–SN50** were obtained after the removal of the protection. The structures of all derivatives were confirmed through ^1H nuclear magnetic resonance (NMR), ^{13}C NMR, and high-resolution mass spectrometry (see Supporting Information for details).

2.2. Anti-biofilm activity and structure–activity relationships analysis

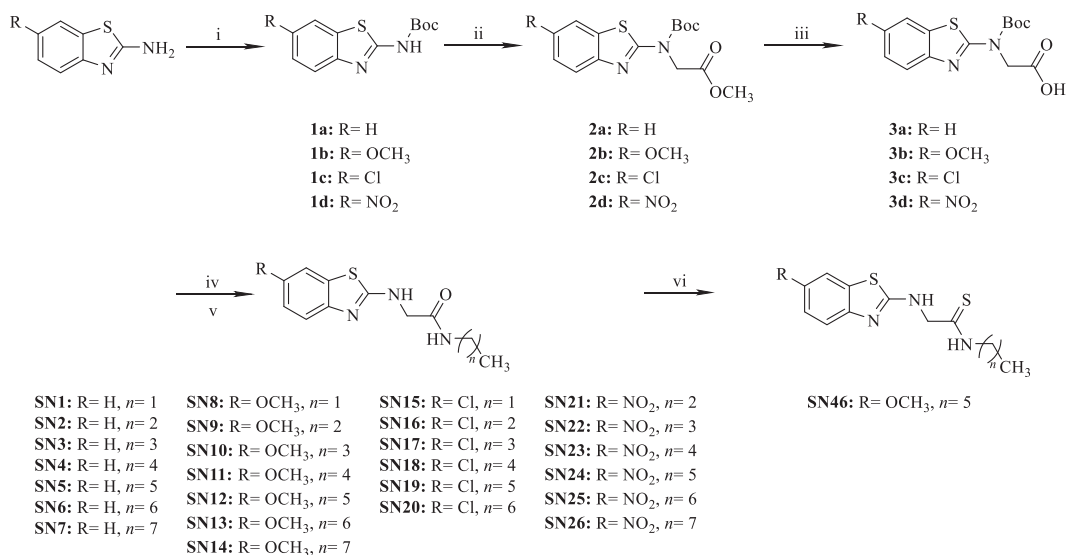
2.2.1. Inhibition of biofilm formation

All derivatives were tested for their anti-biofilm properties. The minimum inhibitory concentration (MIC) assays of the main derivatives **SN1–SN26** were first evaluated, and the results showed that none of these compounds exhibited antimicrobial activity ($\text{MIC} > 256 \mu\text{mol/L}$). In addition, the crystal violet method was used to determine the half inhibitory concentration (IC_{50}) of the biofilm assays for this series of compounds to assess their anti-biofilm potential. We chose Azithromycin (AZM) as a positive control drug, which can broadly inhibit the formation of bacterial biofilms, including *P. aeruginosa*¹⁸. As is shown in Table 1, the results showed that most of compounds had excellent biofilm inhibitory activity ($\text{IC}_{50} < 1 \mu\text{mol/L}$), among which compound **SN12** with methoxy as a substituent and alkyl chain length of 6 had the optimal activity $\text{IC}_{50} = 43 \text{ nmol/L}$.

Chemical structure analysis of the compound **SN12**, which showed the highest inhibitory activity against biofilm formation, led to the synthesis of additional derivatives (**SN27–SN50**). Equally, **SN27–SN50** were subjected to the *P. aeruginosa* anti-microbial assays, which showed that none of these derivatives had anti-*P. aeruginosa* activity ($\text{MIC} > 256 \mu\text{mol/L}$). As shown in Table 2, this series of compounds was used to establish the biofilm inhibitory activity assays and some of the compounds showed anti-biofilm activity. In summary, the majority of the benzothiazole derivatives we synthesized exhibit significant biofilm activity, often surpassing the positive control drug Azithromycin ($\text{IC}_{50} = 9.18 \mu\text{mol/L}$) in potency.

2.2.2. Structure–activity relationships analysis

Based on the biofilm inhibitory activity of all benzothiazole derivatives, the structure–activity relationships were summarized. Firstly, our results confirmed that the introduction of a long alkyl chain increased the biofilm inhibitory concentration of benzothiazoles by an order of magnitude (**SN1–SN26**) compared with previous studies (Table 1). Notably, this increased activity was not observed with the coupling of cyclic moieties (**SN42–SN45**, Table 2). Moreover, the inhibitory activity of compounds with the electron-donating substituent ($-\text{OCH}_3$) was better than that with the electron-withdrawing substituents ($-\text{Cl}$ and $-\text{NO}_2$). The presence of an electron-donating group such as methoxy in **SN12** ($\text{IC}_{50} = 0.04 \mu\text{mol/L}$) resulted in the highest antibiofilm activity, whereas changing the substituent group resulted in decreased anti-biofilm activity. (**SN5**, $\text{IC}_{50} = 0.38 \mu\text{mol/L}$; **SN19**,



Scheme 1 Reagents and conditions: (i) (Boc)₂O, Et₃N, DMAP, DCM, rt, 4 h; (ii) methyl bromoacetate, NaH, dry DMF, 0 °C, 3 h; (iii) NaOH, H₂O, MeOH, 50 °C, 6 h; (iv) Ethylamine-*n*-octylamine, HOBT, EDCi, Et₃N, dry DCM, rt, 6 h; (v) HCl, MeOH, rt, 12 h; (vi) Lawesson reagent, 1,4-dioxane solvent, 90 °C, 12 h.

IC₅₀ = 3.89 μmol/L; **SN24**, IC₅₀ = 2.75 μmol/L). This phenomenon may be attributed to the π-bonding of the aromatic ring's π-electron cloud to the target site, and the presence of the electron-donating substituent enhances the electron cloud of the molecule. It has been observed that the presence of electron-absorbing substituents makes the molecule less soluble.

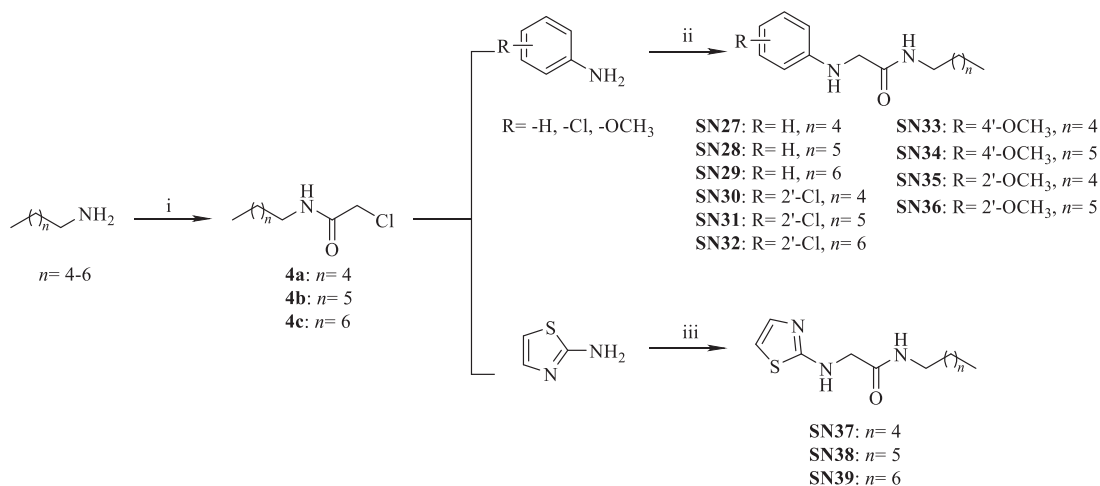
Next, an appropriate increase in the length of the hydrophobic alkyl chain corresponded to an enhancement in the antibiofilm activity of the derivatives (**SN1–SN4**). However, the compounds with excessively long alkyl chains exhibit reduced activity, possibly due to their low solubility and high hydrophobicity (**SN14**, IC₅₀ = 1.01 μmol/L; **SN26**, IC₅₀ = 1.57 μmol/L).

In addition, the splitting of benzothiazole into benzene and thiazole rings (**SN27–SN39**) had a bad effect on biofilm formation. The activity of the compounds was almost entirely lost, except for certain compounds in the thiazole series (**SN38**, IC₅₀ = 4.52 μmol/L).

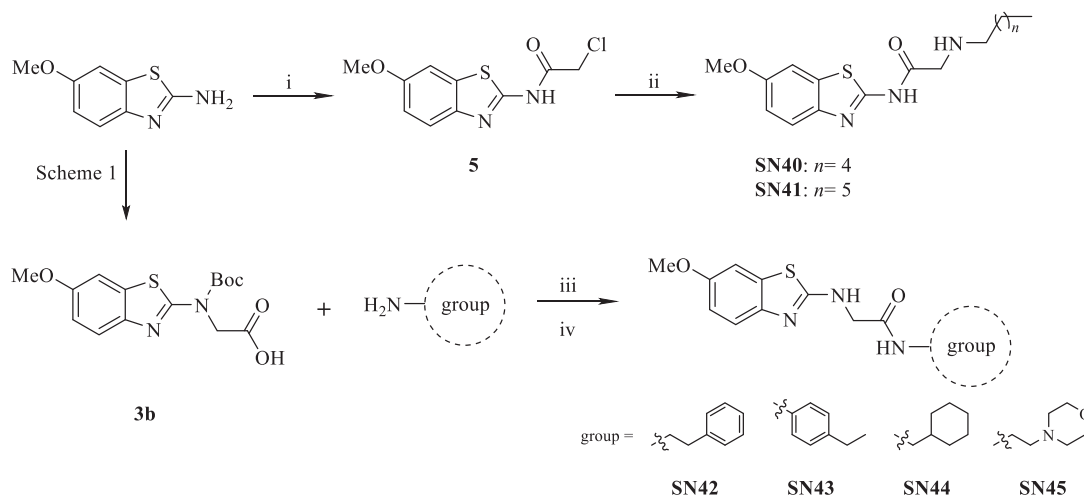
The study demonstrated the ability of benzothiazole to serve as an indispensable pharmacophore for the anti-biofilm activity that was observed. Substitution of electron-donating substituents based on **SN12** was also performed. Given the exceptional activity of **SN12**, our focus in subsequent mechanistic and *in vivo* and *in vitro* activity studies was on this compound.

2.3. Biofilm formation effect of compound **SN12**

Bacteria within biofilms are 10–1000 times more resistant to antibiotics compared with planktonic organisms. The formation of a surface-associated microbial community enables bacteria to survive in the presence of high concentrations of antibiotics, contributing to treatment failure and recurrent infections³³. Effectively limiting the maturation of *P. aeruginosa* biofilm can reduce bacterial resistance to antibiotics³⁴. To determine the effects of the optimally active compound **SN12** (Fig. 2A) on *P.*



Scheme 2 Reagents and conditions: (i) chloroacetyl chloride, K₂CO₃, DCM, 0 °C, 1 h; (ii) K₂CO₃, KI, acetonitrile, 60 °C, 4 h; (iii) K₂CO₃, KI, acetonitrile, 80 °C, 5 h.



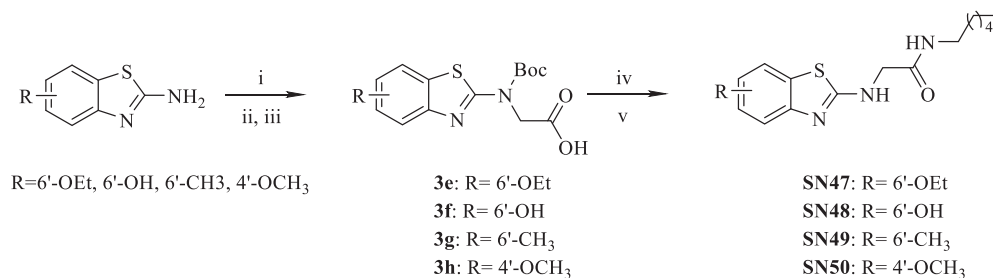
Scheme 3 Reagents and conditions: (i) chloroacetyl chloride, K_2CO_3 , DCM, 0 °C, 1 h; (ii) K_2CO_3 , KI, acetonitrile, 80 °C, 4 h; (iii) amine, HOBT, EDCi, Et_3N , dry DCM, 40 °C, 4 h; (iv) HCl, MeOH, 40 °C, 6 h.

aeruginosa biofilm formation, we employed confocal laser microscopy imaging. The imaging results of compound **SN12** at concentrations of 0.01, 0.1, 1, and 10 $\mu\text{mol/L}$ are depicted in Fig. 2B. The 3D biofilm structure maps revealed that **SN12** could effectively inhibit biofilm formation at a concentration of 10 nmol/L, and it significantly inhibited biofilm formation at 100 nmol/L, compared with the control. The bacterial growth curve profile showed that **SN12** did not inhibit the growth of *P. aeruginosa*, indicating that the compound does not inhibit biofilm formation by suppressing bacterial growth (Fig. 2C). This pronounced disruption of biofilm construction and maturation positions **SN12** as a promising candidate for combating bacterial infections that are resistant to biofilms *in vivo*.

2.4. **SN12** inhibits the expression of genes associated with the two-component system in *P. aeruginosa*

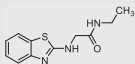
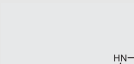
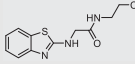
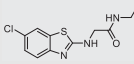
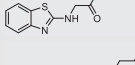
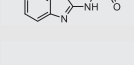
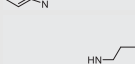
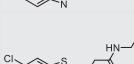
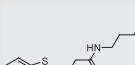
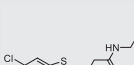
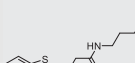
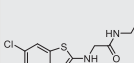
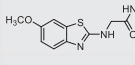
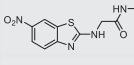
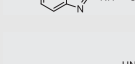
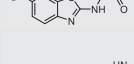
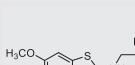
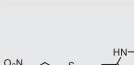
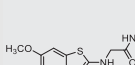
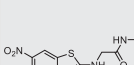
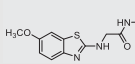
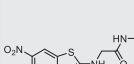


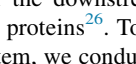
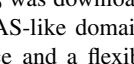
Bacterial biofilm formation is regulated by several mechanisms, such as TCSs, the quorum sensing system, and the bacterial virulence secretion system³⁵. In these mechanisms, proteins play a crucial role in assembling and secreting the fundamental substances that constitute the biofilm. The expression levels of the proteins reflect the level of regulation in the biofilm process⁹. To reveal the targets and mechanisms through which **SN12** may influence biofilm formation, we performed a TMT-tagged quantitative proteomic analysis. *P. aeruginosa* PAO1 was cultured

with or without **SN12**, and total protein was extracted. Differential protein expression was quantified through a comparison of mass spectrometry data. The mass spectrometry proteomics data have been deposited in the ProteomeXchange Consortium with the dataset identifier PXD047035. Drastic changes in protein expression were observed in **SN12**-treated PAO1 compared with the blank group, suggesting that **SN12** affects multifaceted physiological mechanisms. A total of 270 differential proteins were identified in the treated group (fold change [FC] >1.2, $P < 0.05$), of which 124 proteins were downregulated and 146 proteins were upregulated (Fig. 3A). We then analyzed these differential proteins through a KEGG pathway enrichment analysis. As illustrated in Fig. 3B, **SN12** exerted significant effects on the TCSs, oxidative phosphorylation, and biofilm formation pathways. Considering the global regulatory role of TCSs, we hypothesized that **SN12** might act on the TCSs. In a more detailed analysis using a heatmap of differential proteins, GNQ20_17230 (FC = 0.574) and ALP65_01379 (FC = 0.663) emerged as the most significantly downregulated proteins, showing a pronounced decrease of more than 1.5-fold (Fig. 3C). Notably, both proteins belong to the GacS family (former name: LemA) of proteins, indicating that **SN12** may influence the formation of biofilm by interacting with GacS in the TCSs. The GacS protein is a component of the Gac/Rsm system within a TCS that is bidirectionally regulated by the phosphorylated kinases LadS and RetS^{26,36}. Upon signaling activation, GacS



Scheme 4 Reagents and conditions: (i) $(\text{Boc})_2\text{O}$, Et_3N , DMAP, DCM, rt, 4 h; (ii) methyl bromoacetate, NaH, dry DMF, 0 °C, 3 h; (iii) NaOH, H_2O , MeOH, 40 °C, 6 h; (iv) hexylamine, HOBT, EDCi, Et_3N , dry DCM, 40 °C, 4 h; (v) HCl, MeOH, 40 °C, 6 h.

Table 1 Biofilm inhibitory activity and MIC of compounds **SN1**–**SN26** in *P. aeruginosa* PAO1.

Compd.	Structure	IC ₅₀ (μmol/L)	MIC (μmol/L)	Compd.	Structure	IC ₅₀ (μmol/L)	MIC (μmol/L)
SN1		4.24 ± 2.60	>256	SN14		1.01 ± 1.24	>256
SN2		0.68 ± 0.55	>256	SN15		0.98 ± 0.61	>256
SN3		0.39 ± 0.22	>256	SN16		0.92 ± 0.82	>256
SN4		0.33 ± 0.13	>256	SN17		0.27 ± 0.33	>256
SN5		0.38 ± 0.42	>256	SN18		0.20 ± 0.09	>256
SN6		0.18 ± 0.09	>256	SN19		3.89 ± 4.62	>256
SN7		0.17 ± 0.16	>256	SN20		0.43 ± 0.35	>256
SN8		0.26 ± 0.07	>256	SN21		3.01 ± 1.99	>256
SN9		0.16 ± 0.12	>256	SN22		0.28 ± 0.36	>256
SN10		1.29 ± 0.44	>256	SN23		0.82 ± 0.46	>256
SN11		0.55 ± 0.38	>256	SN24		2.75 ± 3.97	>256
SN12		0.04 ± 0.03	>256	SN25		0.19 ± 0.12	>256
SN13		0.05 ± 0.05	>256	SN26		1.57 ± 1.60	>256

transfers the phosphate group to GacA, which regulates the expression of the downstream small RNAs *rsmY* and *rsmZ* by activating the proteins²⁶. To determine the effect of **SN12** on the Gac/Rsm system, we conducted RT-PCR experiments to measure the levels of bacterial expression of relevant genes in the Gac/Rsm system. The results revealed that the treatment of compound **SN12** significantly reduced the expression of *gacS*, *gacA*, *retS*, *ladS*, *rsmY*, and *rsmZ* (Fig. 3D). These findings suggest that compound **SN12** operates on a two-component signaling system, modulating biofilm formation and potentially influencing the Gac/Rsm system.

2.5. *In silico* study of GacS and **SN12** binding

According to the information we obtained from the RT-PCR experiments and the structural information of GacS, an ensemble docking scheme was used to investigate the mechanism of **SN12**

regulating the Gac/Rsm system. The solution NMR structure of GacS_{PD} was downloaded from the PDB database, it is an atypical PDC/PAS-like domain formed by 3 β-sheets and 3 α-helices on one face and a flexible major loop on the other side (Fig. 3E). Research revealed that the putative ligand-binding site is located around the region of the major loop and β3³⁷. However, the flexibility of the loop hindered a regular docking site recognition, here MD simulation was employed first to sample the conformation space of the binding site³⁸. The conformation ensemble generated from a conventional MD simulation explored a great space of the loop conformations and provided the open form of the major loop to accommodate ligands (Fig. 3F). A global binding site search on protein from the trajectory was performed followed the simulation³⁹. Top sites were clustered and screened by both the site score and volume, among the 68 clusters identified, site 22 which appeared 91.6% of the frames was found the most promising for its size (avg. 136.11 Å³) and location. This

Table 2 Biofilm inhibitory activity and MIC of compounds SN27–SN50 in *P. aeruginosa* PAO1.

Compd.	Structure	IC ₅₀ (μmol/L)	MIC (μmol/L)	Compd.	Structure	IC ₅₀ (μmol/L)	MIC (μmol/L)
SN27		> 100	>256	SN40		> 100	>256
SN28		> 100	>256	SN41		> 100	>256
SN29		> 100	>256	SN42		51.06 ± 22.30	>256
SN30		> 100	>256	SN43		> 100	>256
SN31		> 100	>256	SN44		12.65 ± 6.17	>256
SN32		> 100	>256	SN45		> 100	>256
SN33		> 100	>256	SN46		> 100	>256
SN34		> 100	>256	SN47		> 100	>256
SN35		> 100	>256	SN48		42.59 ± 35.35	>256
SN36		20.79 ± 10.48	>256	SN49		41.05 ± 34.68	>256
SN37		51.40 ± 20.67	>256	SN50		> 100	>256
SN38		4.52 ± 3.16	>256	AZM		9.17 ± 2.04	40
SN39		> 100	>256				

site fluctuated a bit during the simulation with the flexible loop but remained a preferred volume and close distance to the key residues Arg94, His97, and His124. Docking was conducted on the representative structures from ensemble⁴⁰. Improved

interaction can be observed with Arg94 (H-bond/ π - π interaction), His97 (π - π interaction), and Thr118 (H-bond). To further verify the stability of the ligand binding also possible ligand-induced conformational changes, MD simulation was performed

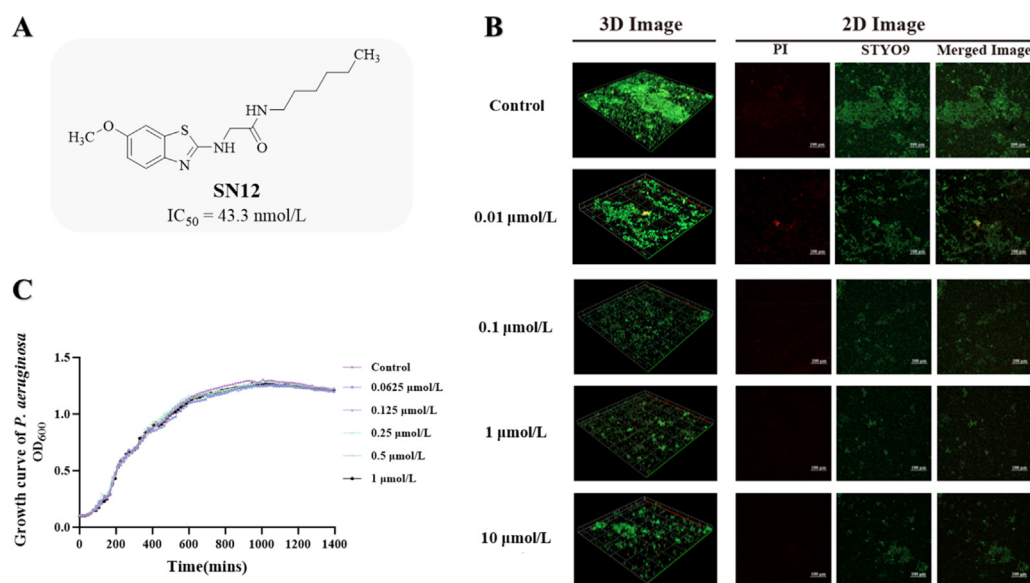


Figure 2 Biofilm formation effects of SN12. (A) Chemical structure of compound SN12. (B) 3D image of *P. aeruginosa* PAO1 biofilm after incubation with SN12 (0.01, 0.1, 1, and 10 μmol/L) for 24 h. (C) Effect of compound SN12 on the real-time growth curve of *P. aeruginosa*. Three independent experiments were performed (for each experiment, $n = 3$).

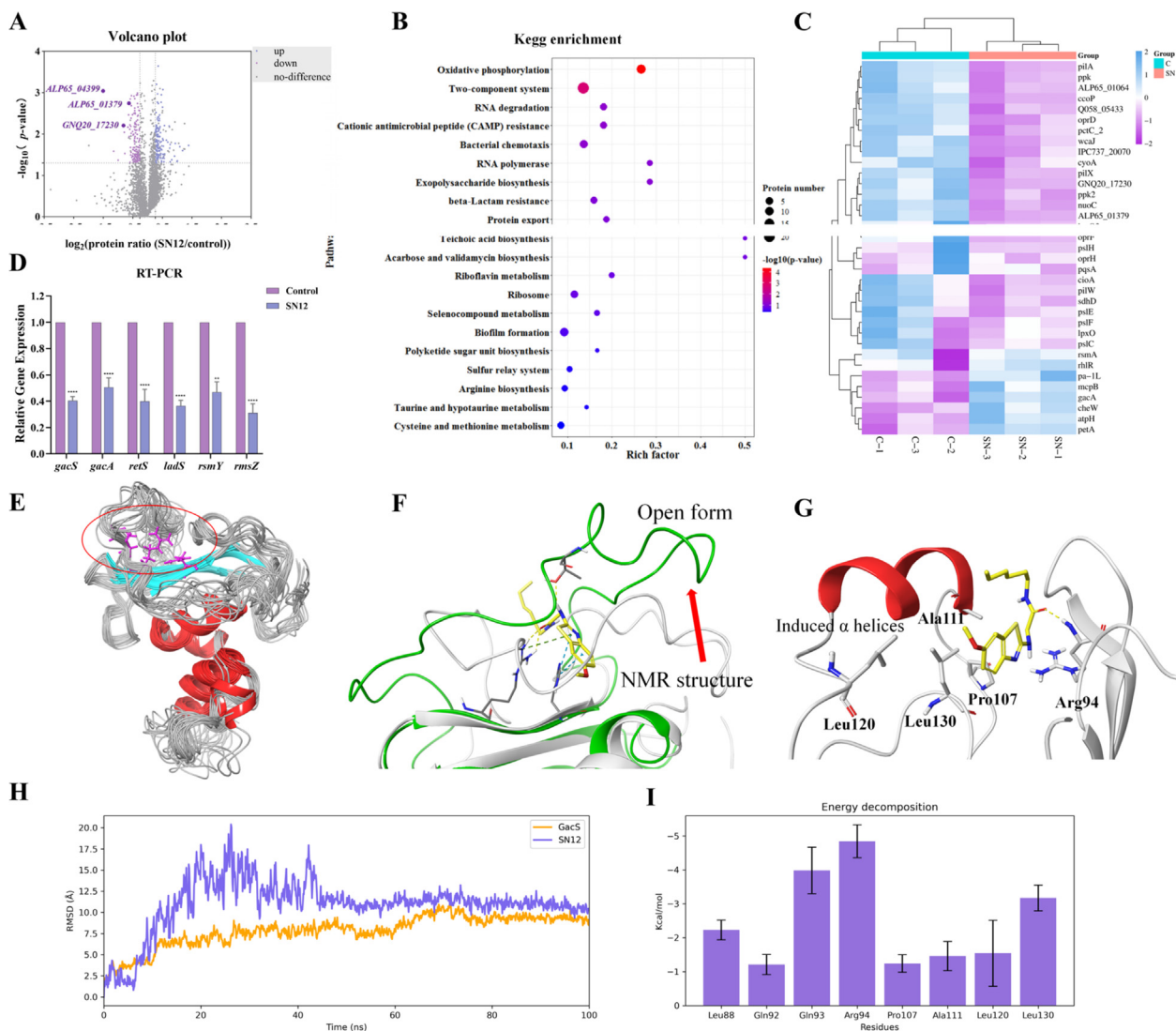


Figure 3 Mechanism analysis of SN12-mediated PAO1 proteomics. (A) Volcano plot was used to screen for differentially expressed proteins between control and SN12 (1000 nmol/L) treatment groups. Slate blue dots indicate up-regulation, purple dots indicate down-regulation and grey dots indicate no-difference-regulation. Dashed lines indicate the screening values satisfy fold change = 1.2, $P = 0.05$. (B) Differential proteins enriched in KEGG pathways. Vertical coordinates are the top 20 pathways significantly enriched, the size of the circle indicates the number of proteins, and the color from green to red indicates the P -value. (C) Heatmap of clustering analysis of selected differentially expressed proteins between control and SN12 treatment groups. (D) RT-PCR experiments results showed compounds SN12 treatment significantly reduced two-component system-related genes at a concentration of 1000 nmol/L. (E) Superimposition of GacS_{PD} representative structures and triad of interacting residues Arg94, His97, and His124. (F) Overlap of original conformation (white) and open form conformation (green) with SN12 docking into site 22. (G) SN12 induced α -helices and the key interacting residues stabilizing the helix (H) RMSD of protein C α and SN12, equilibrium reached in around 50 ns. (I) Energy breakdown on a residue basis. Error bars are equal to \pm SD for three independent replicates, $n = 3$. Using ordinary one-way ANOVA, followed by Tukey's multiple comparison test: * $P \leq 0.05$, ** $P \leq 0.01$, *** $P \leq 0.001$, **** $P \leq 0.0001$.

on the protein-ligand complex⁴¹. During the simulation, key interactions between SN12 and the Arg94 retained for almost every frame (94%) of the equilibrium. The MM/GBSA results from the last 50ns trajectory supported the firm binding for the complex ($\Delta G = -43.46$ kcal/mol with STD 4.09). Notably, the binding of SN12 also induced an extra α -helices from Gly109 to Thr118 and helped stabilize the helices (Fig. 3G and H). Energy breakdown on residue basis gave us an energetical explanation of this process, apart from the major interaction with $\beta 2$ where Arg94 lies, the contribution of residue 107–130 suggested the binding ligand helped to secure the secondary structure by holding the two ends

with hydrophobic interaction, which cannot be observed in the apo-protein simulation (Fig. 3I). In conclusion, our docking and molecular dynamics simulations indicate that SN12 stably binds to the GacS protein ligand site and alters the protein conformation.

Furthermore, we have employed biophysical techniques-microscale thermophoresis (MST) to study the direct interaction between GacS and SN12 *in vitro*. The results, as illustrated in Supporting Information Fig. S1, indicate a direct binding interaction between these two molecules with a dissociation constant (K_d) value of 12.78 ± 0.68 $\mu\text{mol/L}$.

2.6. Compound SN12 combats *P. aeruginosa* biofilm by targeting the Gac/Rsm system

As mentioned, the Gac/Rsm system in TCSs operates as a cascade of top-down regulatory mechanisms²⁷. The level of autophosphorylation between GacS and GacA directly determines downstream changes in regulatory processes⁴². GacA is recognized as a global RR of bacterial physiological behavior and plays a pivotal role in regulating quorum sensing molecules, biofilms, and the secretion of virulence enzymes²¹. To validate our proteomic studies, we conducted further experiments by using the fluorescence reporter strains PAO1-*gacS-gfp* and PAO1-*gacA-gfp* in *P. aeruginosa* treated with SN12. The green fluorescence protein (gfp) gene was integrated downstream from the promoters of *gacS* and *gacA*, and the production of green fluorescent protein (GFP) indicated the activity of these promoters. As illustrated in Supporting Information Fig. S2, no obvious effect on the fluorescence of GFP was observed with compound SN12. However, as depicted in Fig. 4, compound SN12 (0.0625, 0.125, 0.25, 0.5, and 1 $\mu\text{mol/L}$) significantly inhibited the fluorescence of PAO1-*gacS-gfp* (Fig. 4A) and PAO1-*gacA-gfp* (Fig. 4B). These findings indicate that compound SN12 exerts its antibiofilm activity through the Gac/Rsm system in *P. aeruginosa*. Studies have established that the Gac/Rsm system directly activates the transcription of *rsmY* and *rsmZ*²⁶. Thus, we further examined the expression levels of both small RNAs, and the results revealed that SN12 had a certain inhibitory effect on both *rsmZ* (Fig. 4C) and *rsmY* (Fig. 4D). The Gac/Rsm system operates as a closely interconnected entity, and the absence of each component affects the regulation of this global response⁴³. Subsequently, we evaluated how the GacA, RsmY, and RsmZ deficient mutants affect biofilm formation in the presence of SN12. Mutant strains with deleted genes in the Gac/Rsm system showed a reduction in biofilm expression (Supporting Information Fig. S3). Moreover, as depicted in Fig. 4E–G, SN12 demonstrated no anti-biofilm effects on the ΔgacA , ΔrsmY , ΔrsmZ mutants at various concentrations (0.0625, 0.125, 0.25, 0.5, and 1 $\mu\text{mol/L}$). These results suggest that compound SN12 exerts its anti-biofilm activity by targeting the Gac/Rsm system.

The *las* system is a crucial regulatory system for quorum sensing in *P. aeruginosa*, playing key roles in regulating the expression of virulence factors and biofilm formation^{44,45}. Studies on TCSs have demonstrated that the *las* system is directly regulated by Gac/Rsm. When the Gac/Rsm system is inhibited, not only is the synthesis of *las* signaling molecules (3-oxo-C12-HSL) suppressed but also the transcription of *lasR* is repressed (Fig. 4H)⁴³. We further evaluated the effects of SN12 by conducting RT-PCR experiments. Treatment of the bacterial strain PAO1 with SN12 resulted in the downregulation of both *lasR* and *lasB* of the *las* pathway by over 0.5-fold, indicating a significant inhibitory effect of SN12 on the *las* pathway (Fig. 4I). Alternatively, to more thoroughly explore the action of compound SN12 on the *las* pathway, we conducted further experiments by using the fluorescence reporter strains PAO1-*lasB-gfp*, PAO1-*rhlA-gfp*, and PAO1-*pqsA-gfp* in *P. aeruginosa* treated with SN12. The green fluorescence protein (gfp) gene was integrated downstream from the promoters of *lasB*, *rhlA*, and *pqsA*, and the production of GFP indicated the activity of these promoters. As depicted in Fig. 4J, the results revealed that the addition of different doses of compound SN12 significantly reduced the fluorescence values of PAO1-*lasB-gfp*, with the highest reduction

observed when the concentration of compound SN12 was 0.03125 $\mu\text{mol/L}$. This decrease in fluorescence levels was not attributed to compound SN12 acting on fluorescent proteins or altering bacterial growth (Fig. S2 and Fig. 2C). Additionally, the fluorescence values of PAO1-*rhlA-gfp* and PAO1-*pqsA-gfp* were not significantly affected (Supporting Information Fig. S4), which is consistent with the aforementioned regulation of the Gac/Rsm system. The activation of LasR directly regulates the production of virulence factors such as elastase and indirectly regulates the production of virulence factors such as rhamnolipid and pyocyanin. Therefore, we evaluated the effect of SN12 compounds on the production of elastase, pyocyanin, and rhamnolipid. Because the $\Delta\text{lasI}\Delta\text{rhlI}$ double mutant produced very small amounts of elastase, pyocyanin, and rhamnolipid, we selected the $\Delta\text{lasI}\Delta\text{rhlI}$ double mutant as a positive control. Our results indicated that the production of elastase was inhibited in a concentration-dependent manner (Fig. 4K). However, the effect of compound SN12 on the rhamnolipid and pyocyanin contents was not significant (Supporting Information Fig. S5). This finding is consistent with those of the preceding experiments with fluorescent reporter strains, suggesting that SN12 acts as a virulence inhibitor mainly by inhibiting the *las* system. We also monitored the extracellular polysaccharide secretion of *P. aeruginosa* after being treated with the compounds and revealed that the extracellular polysaccharide (*pel/psl* gene) of *P. aeruginosa* was significantly inhibited by SN12 in a concentration-dependent manner (Fig. 4L). These results jointly demonstrated that SN12 can exert biofilm inhibitor effect by inhibiting the *las* quorum sensing system, which is regulated by the Gac/Rsm system of TCSs. These data suggest that SN12 combats biofilm with drug-resistant bacteria by targeting two-component system (Gac/Rsm).

2.7. SN12 inhibits motility and pilus formation in *P. aeruginosa*

Motility is a prominent characteristic of bacteria. Bacteria can exacerbate infections by colonizing the surfaces of objects or infection sites through different modes of movement⁴⁶. Distinct bacterial motility states have been implicated in biofilm formation as well as the development of increased resistance to multiple antibiotics, particularly those based on flagella and IV pili⁴⁷. In *P. aeruginosa*, swarming motility serves as a key indicator of biofilm formation, representing the infection status of the entire bacterial community⁴⁸. During the transition from acute to chronic infection, swarming motility is regulated by TCSs, and swarming motility is significantly impaired in *gacS* mutant strains⁴⁹. Therefore, we evaluated the effects of SN12 on both swarming and swimming motility. The results revealed that SN12 altered the swarming and swimming motility of PAO1 compared with untreated controls (Fig. 5A), prominently inhibiting the swarming motility (Fig. 5B) but exhibiting a slightly less pronounced effect on swimming motility (Fig. 5C). As expected, SN12 demonstrated its regulatory influence on swarming motility through the inhibition of both the Gac/Rsm and the *las* systems. The bacterial flagella and type IV pili (T4P) are pivotal in regulating both swarming and swimming motility; therefore, we further investigated the expression of these components⁵⁰. Proteomic analyses have highlighted a significant downregulation of assembly proteins related to T4P, such as pilA (FC = 0.701) and pilX (FC = 0.742), suggesting that SN12 could influence T4P formation. In RT-PCR experiments, genes associated with pili were also found to be

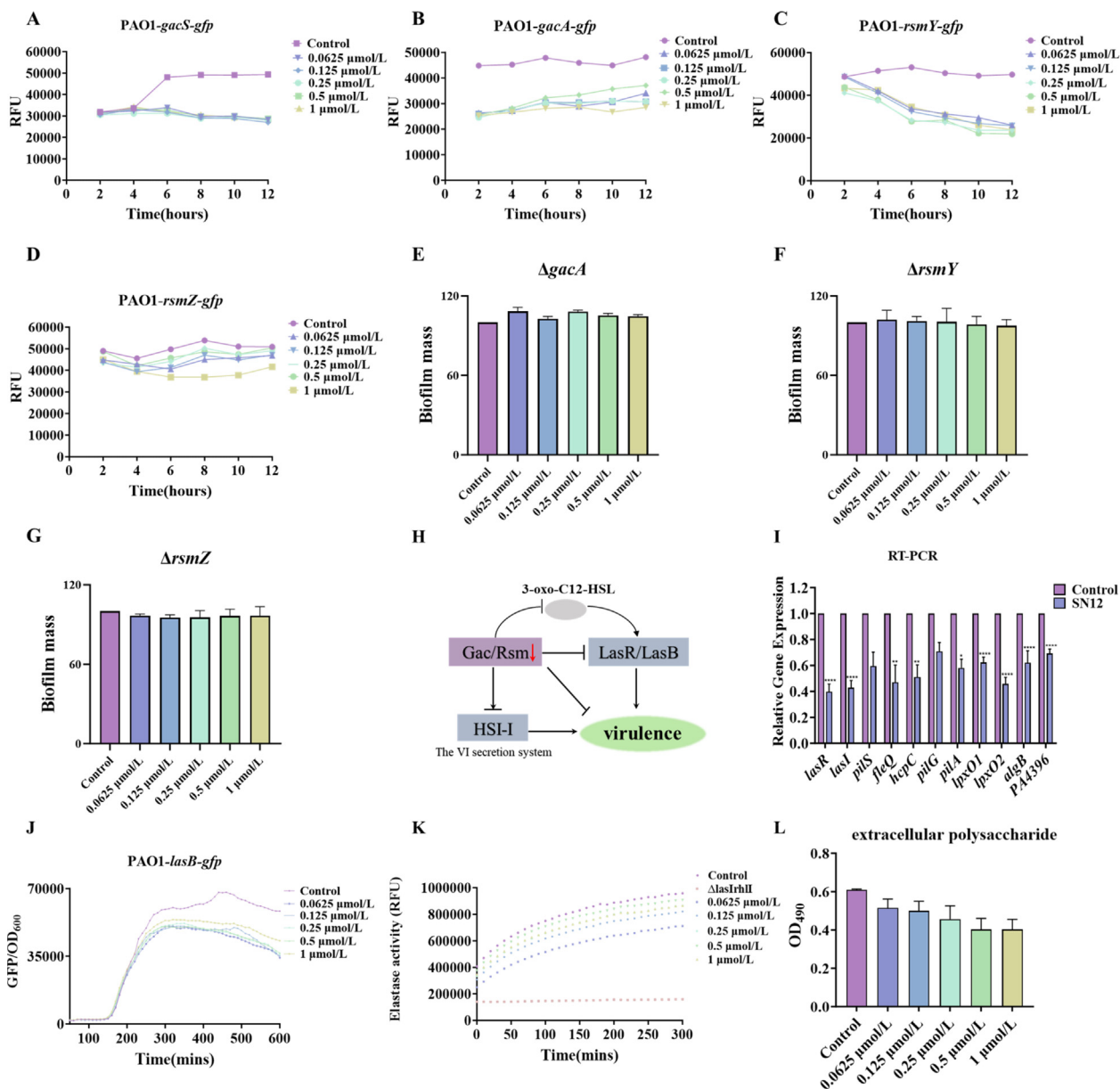


Figure 4 Effect of SN12 on the Gac/Rsm system. (A and B) The effect of measuring compound SN12 on the fluorescence values of PAO1-*gacS-gfp* and PAO1-*gacA-gfp*. (C and D) The effect of measuring compound SN12 on the fluorescence values of *rsmY-gfp* and *rsmZ-gfp*. (E–G) Effect of compound SN12 on biofilm expression of the Gac/Rsm system-related gene deletions (*ΔgacA*, *ΔrsmY*, and *ΔrsmZ*). (H) Mechanisms through which the Gac/Rsm system regulates the expression of bacterial virulence factors. (I) Results of RT-PCR experiments on the genome of PAO1. (J) Effect of SN12 on the expression of *P. aeruginosa* PAO1 fluorescent reporter strain PAO1-*lasB-gfp* and determination of its OD₆₀₀ fluorescence expression for 24 h. (K) Determination of exopolysaccharide expression of PAO1 under incubation with different concentrations of SN12. (L) Effects of total extracellular polysaccharide production by PAO1. Error bars are equal to \pm SD for three independent replicates, $n = 3$. Using ordinary one-way ANOVA, followed by Tukey's multiple comparison test: * $P \leq 0.05$, ** $P \leq 0.01$, *** $P \leq 0.001$, **** $P \leq 0.0001$.

downregulated (Fig. 4I). Furthermore, we evaluated the influence of SN12 on pili formation and confirmed that the pilus formation of *P. aeruginosa* was reduced after treatment with SN12 at concentrations of 0, 0.625, 0.125, 0.25, 0.5, and 1 $\mu\text{mol/L}$, contributing to the inhibition of biofilm formation (Fig. 5D). These results indicate that SN12 may reduce both bacterial motility by inhibiting the Gac/Rsm system and pili formation, thereby affecting early biofilm development and ultimately inhibiting biofilm formation⁵¹.

2.8. Safety evaluations of SN12

To ensure biosafety and assess the potential clinical application, we evaluated the toxicity of the compounds both *in vitro* and *in vivo*. First, we examined the effect of compound SN12 on the human hepatocyte cell line LO2, non-small-cell lung cancer A549 cells, and the human colorectal adenocarcinoma cell line DLD-1 by using the MTT assay. The results revealed that compound SN12 did not exhibit cytotoxicity at concentrations below

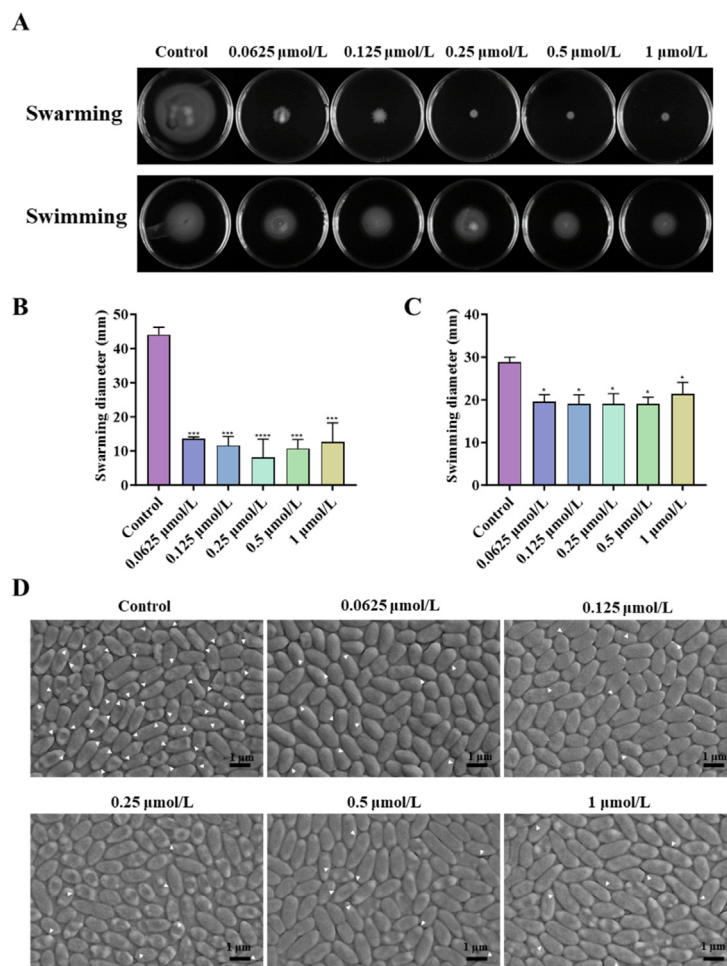


Figure 5 Effects of SN12 on *P. aeruginosa* motility and pilus. (A) Bacterial motility of *P. aeruginosa* under different concentrations of SN12 treatment, including swarming and swimming. (B) Comparison of the diameters of swarming motions in agar plate. (C) Comparison of the diameters of swimming motions in agar plate. (D) Scanning electron micrographs of *P. aeruginosa* at different concentrations of SN12 treatment, legend 1 μm, to observe bacterial pilus and morphology. White filled triangles represent the abundance of pili. Control was untreated. Error bars are equal to ±SD for three independent replicates, $n = 3$. Using ordinary one-way ANOVA, followed by Tukey's multiple comparison tests: $*P \leq 0.05$, $**P \leq 0.01$, $***P \leq 0.001$, $****P \leq 0.0001$.

50 μmol/L (Fig. 6A–C). Second, *in vitro* hemolysis experiments were conducted using red blood cells from two mammalian species, namely, mice and rabbits. The findings indicated that compound SN12 had no hemolytic effect at concentrations below 10 μmol/L, demonstrating a favorable safety profile (Fig. 6D–E). Subsequently, we investigated the effect of compound SN12 on the *in vivo* survival of zebrafish larvae. Zebrafish embryos were treated with varying concentrations of the compound, and the results revealed that the compound had no effect on the survival of zebrafish larvae at concentrations below 200 μmol/L (Fig. 6F). In the *in vitro* and *in vivo* safety evaluation system, SN12 exhibited low toxicity and excellent biocompatibility, making it a promising candidate for drug development.

2.9. SN12 slows the development of ciprofloxacin and tobramycin resistance

Building upon our mechanistic findings, we further investigated the cooperative antimicrobial efficacy of SN12 in conjunction

with ciprofloxacin (Cip) and tobramycin (Tob), aiming to assess their combined therapeutic potential against the multidrug-resistant *P. aeruginosa*. Checkerboard broth microdilution assays were conducted to determine the Fractional Inhibitory Concentration Index (FICI) values, which indicate the level of synergy between SN12 and the antibiotics. The FICI values obtained for SN12 in combination with Cip and Tob were 0.26 and 0.25, respectively (Supporting Information Fig. S6). These values suggest a strong synergistic effect between SN12 and both Cip and Tob, indicating that SN12 enhances the inhibitory activity of these antibiotics *in vitro*. Therefore, based on these findings, SN12 demonstrates the ability to synergize with Cip and Tob in inhibiting bacterial growth *in vitro*, as indicated by the low FICI values observed. These results suggest that SN12 may have therapeutic potential as an adjuvant when combined with Cip and Tob for the treatment of bacterial infections.

The ability of SN12 to impede the development of bacterial resistance is paramount for the therapeutic efficacy of antibiotic combinations; this is because antibiotics introduced in recent

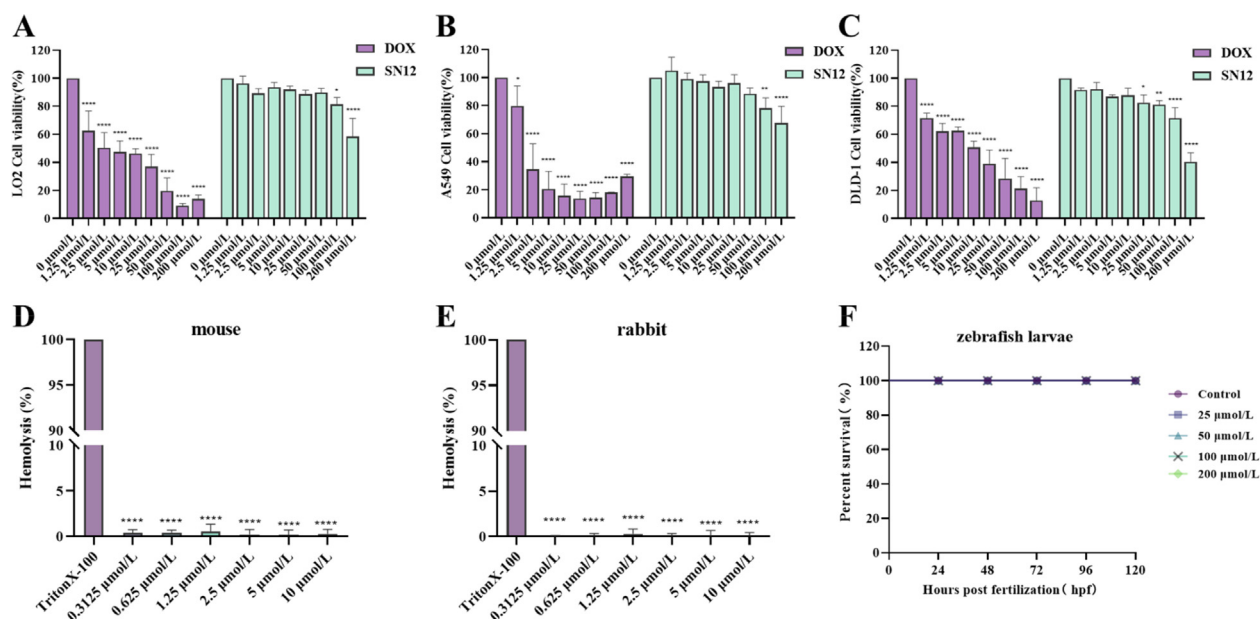


Figure 6 Assessment of *in vitro* toxicity and evaluation of *in vivo* toxicity of SN12. *In vitro* viability of (A) LO2, (B) A549, and (C) DLD-1 cells after being treated with SN12 at various concentrations (0, 1.25, 2.5, 5, 10, 25, 50, 100, 200 μmol/L) for 24 h. Cell viability was determined using an MTT assay. Hemolysis activity of compound SN12 against mouse (D) and rabbit (E) red blood cells. Positive control is TritonX-100 (0.4% *v/v*). (F) *In vivo* toxicity of compound SN12 on development in 3–4 dpf zebrafish larvae at various concentrations (25, 50, 100, and 200 μmol/L). Survival rates were monitored in zebrafish larvae of compound SN12 at various concentrations (25, 50, 100, and 200 μmol/L). Error bars are equal to \pm SD for three independent replicates, $n = 3$. Using ordinary one-way ANOVA, followed by Tukey's multiple comparison test: * $P \leq 0.05$, ** $P \leq 0.01$, *** $P \leq 0.001$, **** $P \leq 0.0001$.

years have been observed to become ineffective within a few months due to bacterial resistance^{52,53}. To determine whether SN12 can mitigate bacterial resistance to Cip and Tob, *P. aeruginosa* PAO1 (ATCC15692) wild-type strain and two multidrug-resistant (MDR) clinical strains (PA3137 and PA1331) were cultured in MH medium containing increasing concentrations of Cip and Tob, with or without SN12 (0.05, 0.1, and 1 μmol/L) at 2 days/cycle. *P. aeruginosa* PAO1 was treated with Cip alone and a combination of Cip and SN12. At the plateau stage, the MIC of the combination of Cip (8 μg/mL) and SN12 was significantly lower than that of Cip alone (128 μg/mL) (Fig. 7A). Two clinical strains of *P. aeruginosa* (PA1313, PA3137) obtained from the First Affiliated Hospital of Jinan University were also assessed. In the case of PA1313 strain, the MIC of the combination of Cip (4 μg/mL) and SN12 was lower than that of Cip alone (128 μg/mL) even at the plateau stage (Fig. 7B). For PA3137 strain, the MIC of the combination of Cip (32 μg/mL) and SN12 was lower than that of Cip alone (256 μg/mL) at the plateau stage (Fig. 7C). Subsequent experiments were conducted to investigate the synergistic effect of SN12 with Tob, another commonly used antibiotic. At the plateau stage, the MIC of the combination of Tob (32 μg/mL) and SN12 was lower than that of Tob alone (64 μg/mL) (Fig. 7D). For PA1313 strain, the MIC of the combination of Tob (64 μg/mL) and SN12 was equivalent to that of Tob alone (64 μg/mL) at the plateau stage (Fig. 7E). For PA3137, at the plateau stage, the MIC of the combination of Tob (32 μg/mL) and SN12 was lower than that of Tob alone (256 μg/mL) (Fig. 7F). These results reveal that compound SN12 can serve as an antibacterial synergist and synergistically resist bacterial resistance with antibiotics. This finding holds potential clinical significance in addressing the challenge of antibiotic resistance.

2.10. SN12 synergizes with ciprofloxacin to attenuate *P. aeruginosa* skin infections *in vivo*

Given SN12's outstanding anti-biofilm activity *in vitro* as well as its exceptional low toxicity and biosafety, we performed *in vivo* anti-infective assays to assess its potential for further development as an anti-infective drug. *P. aeruginosa*, an important microorganism contributing to skin infections in wounds during the development stage and delaying wound healing, was chosen for the study⁷. To simulate the infection scenario, we established a murine exploitative wound skin infection model in BALB/C mice that were infected with *P. aeruginosa*. The bacterial burden was assessed by homogenizing the infected skin lesion and plating the samples on agar plates after 3 days of continuous treatment. Ciprofloxacin (Cip), which is considered a key player in clinical guidelines for treating *P. aeruginosa*, was employed in the study. The use of Cip in a combination antibiotic therapy is driven by considerations of its effectiveness in eradicating *P. aeruginosa* as well as its low cost⁵⁴. To suppress biofilm formation, we evaluated the biofilm inhibition rate of compound SN12 at various concentrations. Our results showed that SN12 had the highest inhibition rate of 70.12% at a concentration of 10 μmol/L (Supporting Information Fig. S7). *In vivo* experiments were performed using SN12 at a concentration of 10 μmol/L, combining the results of its anti-resistance development and *in vitro* co-administration. This result is a crucial reference for selecting the appropriate concentration. The combination therapy strategy of 0.01 mg/mL Cip + 10 μmol/L SN12 and the treatment with 1 mg/mL Cip alone both achieved complete eradication of *P. aeruginosa* (*P. aeruginosa* survival rate: 0%). The mice treated with 0.001 mg/mL Cip and 10 μmol/L SN12 exhibited a

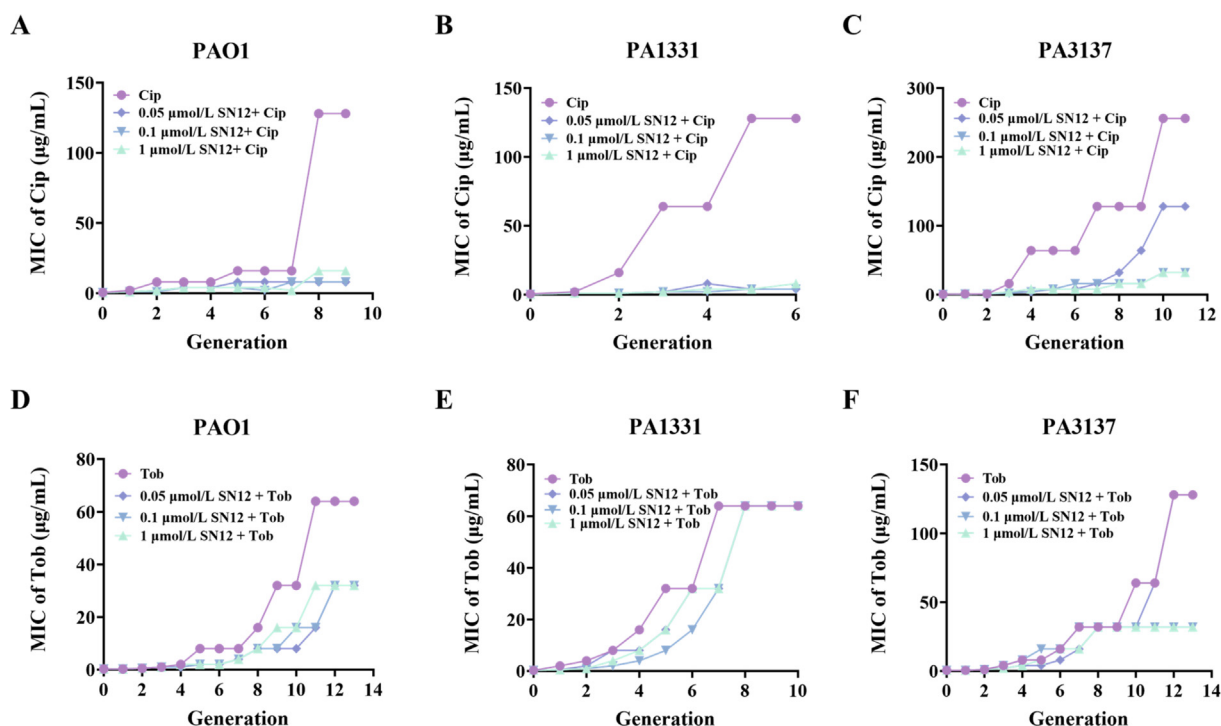


Figure 7 Bacteria are continuously sensitive to **SN12**-enabled antibiotic potentiation. The concentration of Cip/Tob was increased with increasing MIC. The MIC of continuous generation of PAO1 (A), PA3137 (B), and PA1331 (C) in ciprofloxacin, and the effect of continuous passage of PAO1 (D), PA3137 (E), and PA1331 (F) in tobramycin. Cip/Tob indicates antibiotic treatment group alone. Concentration gradient of **SN12**+Cip/Tob indicates the combination treatment group of compounds with antibiotics.

significant reduction in *P. aeruginosa* survival rate (1.66%), inhibiting 98.34% of the bacteria. By contrast, the control group (100%) and the mice treated without **SN12** (0.01 mg/mL Cip: 5.79%, 0.001 mg/mL Cip: 14.74%) exhibited greater bacterial growth (Fig. 8A and B). Additionally, daily monitoring of the wound area underscored the positive synergistic effects of **SN12** when combined with Cip (Fig. 8C and D). In comparisons against a control group, the wound area significantly decreased under the treatment of Cip with or without **SN12** (0.01 mg/mL Cip with or without 10 $\mu\text{mol/L}$ **SN12**, 0.001 mg/mL Cip with or without 10 $\mu\text{mol/L}$ **SN12**). Notably, the combination of 0.001 mg/mL Cip +10 $\mu\text{mol/L}$ **SN12** achieved a nearly comparable healing efficiency (70%) to that of the high-concentration Cip treatment (1 mg/mL). These results indicate that the synergistic effect between compound **SN12** and Cip led to a 1000-fold increase in antibacterial activity.

2.11. **SN12** synergizes with tobramycin and vancomycin to attenuate *P. aeruginosa* skin infections in vivo

We hope that **SN12** offers a comprehensive antimicrobial potentiation effect rather than the mere enhancement of the activity of a single antibiotic. Tobramycin (Tob), commonly prescribed in clinical guidelines for *P. aeruginosa* infections, has demonstrated effectiveness in treating trauma and cystic fibrosis lung infections. However, the emergence of resistance to Tob in various bacteria poses a challenge^{53,56}. Therefore, we selected Tob as a candidate for combination treatment to enhance its dosage and bactericidal effect. In our *in vitro* antimicrobial experiments, the compounds exhibited remarkable antiresistance

activity when used in combination with Tob. As depicted in Fig. 9A and D, the wound treated with 0.005 mg/mL Tob +10 $\mu\text{mol/L}$ **SN12** achieved nearly complete eradication of PAO1, with a bacterial survival rate of only 2.05%, comparable to the bacterial burden in the wound treated with a 100-fold higher dose of Tob (0.5 mg/mL Tob: 0.95%). Similarly, results from an assessment of the wound area corroborated these findings (Fig. 9B and C). The wound treated with 10 $\mu\text{mol/L}$ **SN12** in combination with 0.005 mg/mL Tob exhibited a significantly faster wound healing rate (70.32%) than that treated with 0.5 mg/mL Tob (69.33%) and 0.005 mg/mL Tob (63.01%) alone, and this difference may be attributed to the antibacterial synergistic action of **SN12** inhibiting biofilm formation. In summary, these results indicate that compound **SN12** can enhance the antibacterial efficiency of Tob by 100-fold.

To extend the applicability of **SN12** as a synergistic agent, we replaced Tob with vancomycin (Van), a commonly used antibiotic with less sensitivity to *P. aeruginosa*⁵⁷. As illustrated in Fig. 9E and H, the wound treated with 0.0275 mg/mL Van +10 $\mu\text{mol/L}$ **SN12** achieved near-complete eradication of PAO1, resulting in a bacterial survival rate of 0.8%. This result was comparable to Van treatment at a 200-fold higher dose (5.5 mg/mL Van: 0.08%). Similarly, the wound treated with a combination of 10 $\mu\text{mol/L}$ **SN12** and 0.0275 mg/mL Van (63.06%) exhibited a significantly faster wound healing rate compared with treatment with the low concentration of antibiotics alone (Fig. 9F and G). Thus, these findings indicate that compound **SN12** can enhance the antibacterial efficiency of Van by 200-fold. Experiments assessing the efficacy of antibiotic combinations in eradicating bacteria in skin infections have yielded promising outcomes. Through the

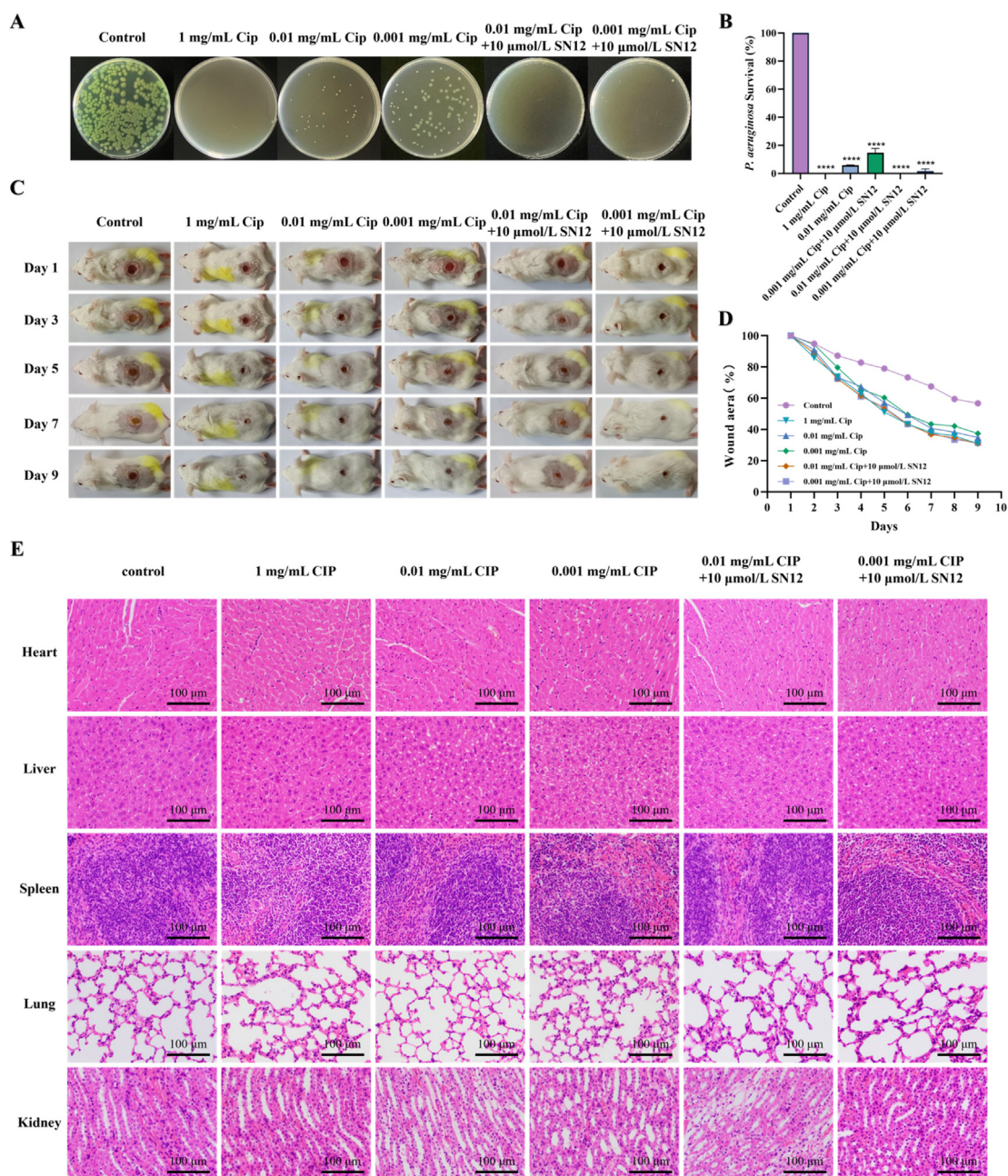


Figure 8 SN12 synergizes with Cip against *P. aeruginosa* infection. (A) The results of CFU counting on agar plates in mice that treated with physiological saline (control), Cip (1 mg/mL, 0.01 mg/mL, 0.001 mg/mL), Cip (0.01 mg/mL) + SN12 (10 μ mol/L), and the Cip (0.001 mg/mL) + SN12 (10 μ mol/L) combination. CFU, colony-forming units. (B) *P. aeruginosa* PAO1 survival rate of wounds. (C) Representative images of wounds during the experiment. (D) The wound area of mice was calculated with *ImageJ* software. (E) Effects of SN12 in combination with Ciprofloxacin on the heart, liver, spleen, lung, and kidney of BALB/C mice. Error bars are equal to \pm SD for three independent replicates, $n = 3$. Using ordinary one-way ANOVA, followed by Tukey's multiple comparison test: * $P < 0.05$, ** $P < 0.01$, *** $P < 0.001$, **** $P < 0.0001$.

inhibition of biofilm formation, SN12 can enhance the effectiveness of various commonly prescribed antibiotics. Notably, SN12 also markedly potentiated the efficacy of the Gram-positive bacterial antibiotic Van, even in cases where the antibiotic was not susceptible to *P. aeruginosa*⁵⁸.

To assess the *in vivo* toxicity of compound SN12 in mice, we measured the body weight of mice at regular time intervals and euthanized them after 9 days. Subsequently, the major organs were extracted and analyzed through hematoxylin and eosin

staining. The results revealed that SN12, when combined with conventional antibiotics including Cip, Tob, and Van, had no significant effect on the heart, liver, spleen, lung, or kidney (Fig. 8E, Supporting Information Figs. S8 and S9) or body weight (Supporting Information Fig. S10) of mice. In summary, SN12 exhibited potent antibacterial synergist activity with low toxicity in a mouse wound infection model. These findings suggest that SN12 holds promise for further development as a synergistic antibacterial drug.

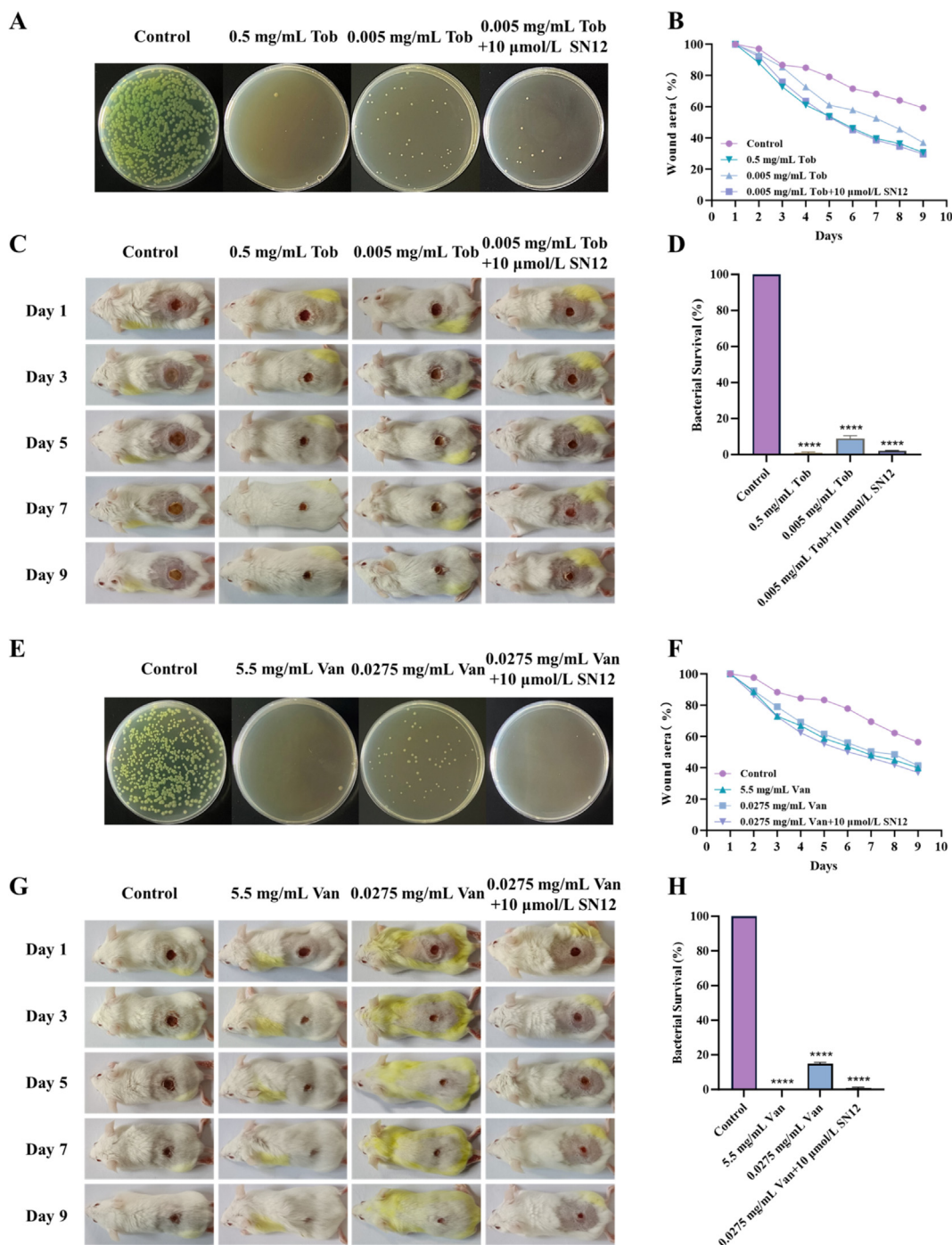


Figure 9 SN12 synergizes with Tob and Van against *P. aeruginosa* infection. (A) The results of CFU counting on agar plates in mice that treated with physiological saline (control), Tob (0.5 mg/mL, 0.005 mg/mL), Tob (0.005 mg/mL) + SN12 (10 μmol/L) combination. CFU, colony-forming units. (B) The wound area of mice was calculated with ImageJ software. (C) Representative images of wounds during the experiment. (D) *P. aeruginosa* PAO1 survival rate of wounds. (E) The results of CFU counting on agar plates in mice that treated with physiological saline (control), Van (5.5 mg/mL, 0.0275 mg/mL), Van (0.0275 mg/mL) + SN12 (10 μmol/L) combination. (F) The wound area of mice was calculated with ImageJ software. (G) Representative images of wounds during the experiment. (H) *P. aeruginosa* PAO1 survival rate of wounds. Error bars are equal to \pm SD for three independent replicates, $n = 3$. Using ordinary one-way ANOVA, followed by Tukey's multiple comparison test: * $P \leq 0.05$, ** $P \leq 0.01$, *** $P \leq 0.001$, **** $P \leq 0.0001$.

3. Conclusions

P. aeruginosa infections pose considerable challenges due to the emergence of biofilm resistance. Since biofilm formation is a key

mechanism of drug resistance in bacteria, researchers are exploring alternative, nonbiocidal approaches to treat and clear bacterial infections^{3,54}. Many chronic infections persistently exhibit drug resistance and are closely linked to bacterial biofilm formation.

Adopting an “anti-biofilm” strategy is crucial in this regard, as it can reduce antibiotic usage and curb the generation and spread of antibiotic resistance^{56,59}. In this study, we designed and synthesized potential biofilm inhibitors by combining benzothiazole with quorum sensing signal molecules, specifically *N*-acyl-homoserine lactone (AcyL-HSL) and *N*-(3-oxo-dodecanoyl)-L-homoserine lactone (OdDHL)’s amide side chain. A newly identified benzothiazole derivative, denoted as **SN12** ($IC_{50} = 43.3$ nmol/L), exhibited remarkable biofilm inhibition at nanomolar concentration *in vitro*. These promising findings highlight the development of **SN12** as a novel and feasible strategy for creating effective biofilm inhibitors for the treatment of *P. aeruginosa* infections in the future. Furthermore, mechanism studies were described, and the effects of this compound **SN12** displayed specific inhibition of two-component (Gac/Rsm) system to strongly repress *gacS*, *gacA*, *rsmY*, and *rsmZ* biosynthesis. Notably, **SN12** demonstrates the ability to reduce the production of biofilm-associated virulence factors. What’s more, we observed a remarkable synergistic effect of **SN12** when combined with Cip, resulting in a 1000-fold enhancement in antibacterial activity in the murine skin wound infection model. Additionally, **SN12** increased the antibacterial activity of Van by over 200-fold and Tob by more than 100-fold in a murine skin wound model of *P. aeruginosa* infection.

This study preliminarily elucidates the initial activity of **SN12** and its combined therapeutic effect against *Pseudomonas aeruginosa*. However, information about the *in vivo* parameters such as pharmacokinetics and tissue distribution of **SN12** is still limited. Furthermore, there is limited information about the efficacy of **SN12** in combination with other classes of antibiotics and its potential to inhibit other infection models. Therefore, future research should focus on investigating the regulatory mechanisms of **SN12**, conducting comprehensive evaluations of its *in vivo* efficacy and safety, optimizing its combination with antibiotics, and exploring the optimal therapeutic strategies. Anyway, these findings emphasize the promise of **SN12** as a lead compound and advocate for future investigations into the development of novel antimicrobial synergists that target this two-component (Gac/Rsm) system to combat bacterial infections.

4. Experimental

4.1. Reagents

All reagents and solvents were commercially purchased and used directly without further purification unless otherwise stated. ¹H NMR and ¹³C NMR spectra of compounds were recorded using a 400 MHz NMR spectrometer (Bruker DRX400), and the products were solubilized with deuterated DMSO or deuterated methanol reagent, and data acquisition was carried out under a stable magnetic field, with deuterated reagent from Energy Chemica Ltd. HRMS spectra were confirmed on a Finnigan MAT-90 spectrometer or an Agilent 6210 series LC/MSD TOF mass spectrometer, and the products were solubilized with chromatographic methanol solvent, filtered through a 0.2–0.5 μm filter membrane, and then subjected to data acquisition in either positive or negative ion mode. The results of HRMS spectra are shown in [Supporting Information Table S3](#). HPLC was used for purity analysis (Thermo Scientific Dionex Ultimate 3000 series) with a reversed-phase C18 column, and chromatography grade methanol and ultrapure water were used as mobile phase eluents. The purity of all biologically tested compounds was determined by HPLC >95% ([Supporting Information Table S2](#)).

4.2. General procedure for the synthesis of intermediate **3a**

4.2.1. *Tert*-butyl benzo[d]thiazol-2-ylcarbamate (**1a**)

2-Aminobenzothiazole (0.01 mol) was dissolved in dichloromethane. The reaction was maintained by the addition of triethylamine (0.02 mol) and DMAP (0.0002 mol) and then kept stirring at room temperature, followed by the dropwise addition of (Boc)₂O (0.012 mol). And the reaction was terminated with the continuation of the reaction for about 4 h after the completion of solvent dropwise addition. The residual organic solvent in the reaction system was removed, then recrystallized with petroleum ether/ethyl acetate (48:2) and filtered under reduced pressure to obtain a grey solid as intermediate **1a** in 85% yield. ¹H NMR (400 MHz, DMSO-*d*₆) δ 11.74 (s, 1H), 7.92 (d, *J* = 7.9 Hz, 1H), 7.70–7.63 (m, 1H), 7.39 (t, *J* = 7.7 Hz, 1H), 7.28–7.22 (m, 1H), 1.51 (d, *J* = 2.1 Hz, 9H). ¹³C NMR (101 MHz, DMSO) δ 160.05, 153.41, 149.53, 132.56, 126.46, 123.61, 121.89, 120.61, 82.28, 28.31.

4.2.2. Methyl *N*-(benzo[d]thiazol-2-yl)-*N*-(*tert*-butoxycarbonyl)glycinate (**2a**)

Intermediate **1a** (0.01 mol) was placed in a 50 mL two-necked flask and dissolved with appropriate amount of anhydrous DMF. Sodium hydride (0.012 mol) was added and stirred at 0 °C for 30 min, followed by the addition of methyl bromoacetate (0.011 mol) dropwise. The reaction was continued for about 2 h and then quenched by adding a small amount of ice water. The organic phases were extracted with 100 mL × 3 ethyl acetate and combined, followed by washing with 100 mL × 3 saturated NH₄Cl solution and 100 mL × 3 saturated NaCl solution until the effluent aqueous layer was neutral. After sufficient drying with MgSO₄ and filtration, the solvent was removed and the residue was purified by fast chromatography (petroleum ether-ethyl acetate = 80/20 *v/v*) to give a white solid as intermediate **2a** in 70% yield. ¹H NMR (400 MHz, chloroform-*d*) δ 7.87–7.72 (m, 2H), 7.40 (ddd, *J* = 8.4, 7.3, 1.3 Hz, 1H), 7.30–7.26 (m, 1H), 5.01 (s, 2H), 3.79 (s, 3H), 1.60 (s, 9H). ¹³C NMR (101 MHz, CDCl₃) δ 169.12, 160.52, 148.80, 133.67, 133.41, 125.78, 123.51, 121.20, 120.82, 77.24, 52.31, 48.10, 28.08.

4.2.3. *N*-(Benzo[d]thiazol-2-yl)-*N*-(*tert*-butoxycarbonyl)glycine (**3a**)

Intermediate **2a** (0.01 mol) was dissolved in methanol, and the reaction was terminated by adding 2 N aqueous sodium hydroxide solution (containing 0.02 mol of sodium hydroxide) and stirring at 50 °C for 6 h. After Removing methanol, adjusting its pH to 5 with 1 mol/L HCl, the solid was precipitated, filtered under reduced pressure and dried in vacuum, a white solid was obtained as intermediate **3a**, yield: 90%. **3b–3h** were prepared as in **3a**. ¹H NMR (400 MHz, DMSO-*d*₆) δ 12.88 (s, 1H), 7.95 (d, *J* = 7.9 Hz, 1H), 7.73 (d, *J* = 8.2 Hz, 1H), 7.42 (t, *J* = 7.8 Hz, 1H), 7.30 (t, *J* = 7.7 Hz, 1H), 4.83 (s, 2H), 1.52 (s, 9H). ¹³C NMR (101 MHz, DMSO) δ 169.95, 169.09, 160.79, 148.80, 133.32, 126.59, 124.18, 121.91, 121.23, 52.75, 48.33, 28.03.

4.3. General procedure for the synthesis of target compounds **SN1** to **SN26**

4.3.1. 2-(Benzo[d]thiazol-2-ylamino)-*N*-ethylacetamide (**SN1**)

Intermediate **3a** (0.60 mmol, 1.0 equiv) was dissolved in dichloromethane, 1-hydroxybenzotriazole (HOBT, 0.72 mmol, 1.2 equiv) and Et₃N (1.20 mmol, 2.0 equiv) were added and the

reaction was stirred at room temperature for 30 min, and then the reaction was terminated by the addition of EDCI (0.72 mmol, 1.2 equiv) and ethylamine (0.72 mmol, 1.2 equiv) after 6 h of reaction. The reaction solution was extracted with EtOAc (30 mL \times 3), washed with NaHCO₃ solution, NH₄Cl solution and saturated NaCl solution, respectively, until the neutral pH. The combined organic phases were sufficiently dried with MgSO₄ and then filtered, and the solvent was removed in vacuum to obtain a white solid as the crude intermediate. The reaction was terminated by placing intermediate in 6 mol/L HCl in methanol solution with stirring for 12 h at room temperature. The reaction solution was adjusted to pH 7 with 1 mol/L NaOH, methanol was removed and extracted with EtOAc (30 mL \times 3), the organic phase was dried and the solvent was removed. The crude product was purified by flash chromatography (petroleum/EtOAc, 1:1). The pure product was collected as a white solid **SN1** (67.5 mg, yield: 47.8%). ¹H NMR (400 MHz, DMSO-*d*₆) δ 8.46 (s, 1H), 8.15 (d, *J* = 5.9 Hz, 1H), 7.67 (d, *J* = 7.9 Hz, 1H), 7.38 (d, *J* = 8.2 Hz, 1H), 7.22 (t, *J* = 7.4 Hz, 1H), 7.02 (t, *J* = 7.5 Hz, 1H), 3.98 (s, 2H), 3.11 (d, *J* = 6.5 Hz, 2H), 1.03 (t, *J* = 7.1 Hz, 3H). ¹³C NMR (101 MHz, DMSO-*d*₆) δ 168.86, 166.74, 152.68, 131.14, 125.91, 121.47, 121.39, 118.54, 47.12, 33.89, 15.19. HRMS (ESI) of compound **SN1**: calcd for C₁₁H₁₃N₃OS [M + H]⁺ = 236.0853, found [M + H]⁺ = 236.0866.

4.3.2. 2-(Benzo[d]thiazol-2-ylamino)-N-propylacetamide (SN2)
The compound was prepared with reference to compound **SN1** using intermediate **3a** (0.60 mmol, 1.0 equiv) and *n*-propylamine (0.72 mmol, 1.2 equiv) as raw material. The pure product was collected to give white solid **SN2** (77.5 mg, yield: 51.8%). ¹H NMR (400 MHz, DMSO-*d*₆) δ 8.93 (t, *J* = 5.6 Hz, 1H), 7.99 (d, *J* = 7.9 Hz, 1H), 7.71–7.12 (m, 3H), 5.22 (s, 2H), 3.06 (q, *J* = 6.5 Hz, 2H), 1.45 (h, *J* = 7.1 Hz, 2H), 0.86 (t, *J* = 7.3 Hz, 3H). ¹³C NMR (101 MHz, DMSO-*d*₆) δ 169.23, 164.45, 138.88, 128.15, 125.59, 123.99, 122.72, 113.19, 47.77, 41.16, 22.58, 11.86. HRMS (ESI) of compound **SN2**: calcd for C₁₂H₁₅N₃OS [M + H]⁺ = 250.1009, found [M + H]⁺ = 250.1016.

4.3.3. 2-(Benzo[d]thiazol-2-ylamino)-N-butylacetamide (SN3)
The compound was prepared with reference to compound **SN1** using intermediate **3a** (0.60 mmol, 1.0 equiv) and *n*-butylamine (0.72 mmol, 1.2 equiv) as raw material. The pure product was collected to give white solid **SN3** (78.1 mg, yield: 49.4%). ¹H NMR (400 MHz, Methanol-*d*₄) δ 8.19 (s, 1H), 7.82 (d, *J* = 8.0 Hz, 1H), 7.70 (d, *J* = 8.1 Hz, 1H), 7.39 (t, *J* = 7.8 Hz, 1H), 7.27 (t, *J* = 7.7 Hz, 1H), 3.25 (q, *J* = 6.8 Hz, 2H), 1.53 (t, *J* = 7.5 Hz, 2H), 1.37 (ddd, *J* = 32.7, 16.2, 6.8 Hz, 4H), 0.95 (p, *J* = 5.3, 4.9 Hz, 3H). ¹³C NMR (101 MHz, DMSO-*d*₆) δ 169.01, 166.75, 152.58, 131.04, 126.00, 121.61, 121.41, 118.57, 47.08, 38.70, 31.60, 19.90, 14.08. HRMS (ESI) of compound **SN3**: calcd for C₁₃H₁₇N₃OS [M + H]⁺ = 264.1166, found [M + H]⁺ = 264.1178.

4.3.4. 2-(Benzo[d]thiazol-2-ylamino)-N-pentylacetamide (SN4)
The compound was prepared with reference to compound **SN1** using intermediate **3a** (0.60 mmol, 1.0 equiv) and *n*-amylamine (0.72 mmol, 1.2 equiv) as raw material. The pure product was collected to give white solid **SN4** (88.5 mg, yield: 53.2%). ¹H NMR (400 MHz, DMSO-*d*₆) δ 8.23 (t, *J* = 5.6 Hz, 1H), 7.97 (t, *J* = 5.6 Hz, 1H), 7.67 (dd, *J* = 7.8, 1.3 Hz, 1H), 7.37 (d, *J* = 8.2 Hz, 1H), 7.21 (td, *J* = 7.7, 1.4 Hz, 1H), 7.02 (td, *J* = 7.6, 1.3 Hz, 1H), 3.98 (d, *J* = 5.6 Hz, 2H), 3.08 (q, *J* = 6.6 Hz, 2H),

1.40 (p, *J* = 6.9 Hz, 2H), 1.33–1.18 (m, 4H), 0.83 (t, *J* = 6.7 Hz, 3H). ¹³C NMR (101 MHz, DMSO-*d*₆) δ 168.95, 166.72, 152.63, 131.09, 125.96, 121.57, 121.39, 118.57, 47.12, 38.98, 29.20, 28.97, 22.29, 14.32. HRMS (ESI) of compound **SN4**: calcd for C₁₄H₁₉N₃OS [M + H]⁺ = 278.1322, found [M + H]⁺ = 278.1336.

4.3.5. 2-(Benzo[d]thiazol-2-ylamino)-N-hexylacetamide (SN5)
The compound was prepared with reference to compound **SN1** using intermediate **3a** (0.60 mmol, 1.0 equiv) and *n*-hexylamine (0.72 mmol, 1.2 equiv) as raw material. The pure product was collected to give white solid **SN5** (83.1 mg, yield: 47.5%). ¹H NMR (400 MHz, DMSO-*d*₆) δ 8.23 (t, *J* = 5.6 Hz, 1H), 7.96 (t, *J* = 5.5 Hz, 1H), 7.67 (d, *J* = 7.8 Hz, 1H), 7.37 (d, *J* = 7.8 Hz, 1H), 7.21 (t, *J* = 7.6 Hz, 1H), 7.02 (t, *J* = 7.4 Hz, 1H), 3.98 (d, *J* = 5.7 Hz, 2H), 3.08 (q, *J* = 6.5 Hz, 2H), 1.39 (t, *J* = 6.9 Hz, 2H), 1.31–1.15 (m, 6H), 0.83 (t, *J* = 6.2 Hz, 3H). ¹³C NMR (101 MHz, DMSO-*d*₆) δ 168.88, 166.67, 152.67, 131.13, 125.91, 121.50, 121.39, 118.55, 47.08, 39.00, 31.46, 29.52, 26.48, 22.51, 14.37. HRMS (ESI) of compound **SN5**: calcd for C₁₅H₂₁N₃OS [M + H]⁺ = 292.1479, found [M + H]⁺ = 292.1486.

4.3.6. 2-(Benzo[d]thiazol-2-ylamino)-N-heptylacetamide (SN6)
The compound was prepared with reference to compound **SN1** using intermediate **3a** (0.60 mmol, 1.0 equiv) and *n*-heptanamine (0.72 mmol, 1.2 equiv) as raw material. The pure product was collected to give white solid **SN6** (90.5 mg, yield: 49.4%). ¹H NMR (400 MHz, DMSO-*d*₆) δ 8.24 (t, *J* = 5.8 Hz, 1H), 7.96 (t, *J* = 5.7 Hz, 1H), 7.67 (dd, *J* = 7.9, 1.2 Hz, 1H), 7.37 (dd, *J* = 8.1, 1.1 Hz, 1H), 7.22 (td, *J* = 7.7, 1.3 Hz, 1H), 7.03 (td, *J* = 7.5, 1.2 Hz, 1H), 3.98 (d, *J* = 5.6 Hz, 2H), 3.08 (q, *J* = 6.6 Hz, 2H), 1.40 (t, *J* = 6.9 Hz, 2H), 1.23 (q, *J* = 6.5, 5.3 Hz, 8H), 0.90–0.79 (m, 3H). ¹³C NMR (101 MHz, DMSO-*d*₆) δ 168.89, 166.67, 152.68, 131.14, 125.91, 121.50, 121.39, 118.55, 47.10, 38.98, 31.71, 29.56, 28.91, 26.76, 22.52, 14.41. HRMS (ESI) of compound **SN6**: calcd for C₁₆H₂₃N₃OS [M + H]⁺ = 306.1635, found [M + H]⁺ = 306.1643.

4.3.7. 2-(Benzo[d]thiazol-2-ylamino)-N-octylacetamide (SN7)
The compound was prepared with reference to compound **SN1** using intermediate **3a** (0.60 mmol, 1.0 equiv) and *n*-octylamine (0.72 mmol, 1.2 equiv) as raw material. The pure product was collected to give white solid **SN7** (97.2 mg, yield: 50.8%). ¹H NMR (400 MHz, methanol-*d*₄) δ 7.61 (d, *J* = 8.0 Hz, 1H), 7.46 (d, *J* = 8.2 Hz, 1H), 7.27 (t, *J* = 7.8 Hz, 1H), 7.09 (t, *J* = 7.6 Hz, 1H), 4.08 (d, *J* = 6.0 Hz, 2H), 3.28–3.09 (m, 2H), 1.50 (q, *J* = 7.0 Hz, 2H), 1.26 (d, *J* = 12.7 Hz, 10H), 0.89 (t, *J* = 6.7 Hz, 3H). ¹³C NMR (101 MHz, MeOD-*d*₄) δ 170.19, 166.61, 151.66, 130.38, 125.48, 121.62, 120.47, 118.12, 46.72, 39.04, 31.56, 29.02, 29.00, 28.96, 26.54, 22.29, 13.00. HRMS (ESI) of compound **SN7**: calcd for C₁₇H₂₅N₃OS [M + H]⁺ = 320.1792, found [M + H]⁺ = 320.1809.

4.3.8. N-Ethyl-2-((6-methoxybenzo[d]thiazol-2-yl)amino)acetamide (SN8)

The compound was prepared with reference to compound **SN1** using intermediate **3b** (0.60 mmol, 1.0 equiv) and ethylamine (0.72 mmol, 1.2 equiv) as raw material. The pure product was collected to give white solid **SN8** (87.1 mg, yield: 54.7%). ¹H NMR (400 MHz, methanol-*d*₄) δ 7.37 (d, *J* = 8.8 Hz, 1H), 7.23 (t, *J* = 2.3 Hz, 1H), 6.89 (dd, *J* = 8.8, 2.6 Hz, 1H), 4.07 (s, 2H), 3.81 (s, 3H), 3.27 (q, *J* = 7.2 Hz, 2H), 1.14 (t, *J* = 7.3 Hz, 3H). ¹³C

NMR (101 MHz, MeOD- d_4) δ 170.12, 166.03, 155.58, 145.73, 131.38, 118.48, 113.16, 104.98, 54.91, 46.68, 33.90, 13.48. HRMS (ESI) of compound **SN8**: calcd for $C_{12}H_{15}N_3O_2S$ [M + H]⁺ = 266.0958, found [M + H]⁺ = 266.0955.

4.3.9. 2-((6-Methoxybenzo[d]thiazol-2-yl)amino)-*N*-propylacetamide (**SN9**)

The compound was prepared with reference to compound **SN1** using intermediate **3b** (0.60 mmol, 1.0 equiv) and *n*-propylamine (0.72 mmol, 1.2 equiv) as raw material. The pure product was collected to give white solid **SN9** (89.0 mg, yield: 53.1%). ¹H NMR (400 MHz, DMSO- d_6) δ 7.99 (dt, J = 20.6, 6.4 Hz, 2H), 7.36–7.22 (m, 2H), 6.86–6.77 (m, 1H), 3.99–3.89 (m, 2H), 3.74 (d, J = 2.5 Hz, 3H), 3.05 (q, J = 6.9 Hz, 2H), 1.42 (q, J = 7.5 Hz, 2H), 0.84 (td, J = 7.6, 2.3 Hz, 3H). ¹³C NMR (101 MHz, DMSO- d_6) δ 169.07, 165.10, 154.88, 146.73, 132.14, 118.90, 113.40, 106.01, 55.99, 47.09, 40.78, 22.82, 11.79. HRMS (ESI) of compound **SN9**: calcd for $C_{13}H_{17}N_3O_2S$ [M + H]⁺ = 280.1115, found [M + H]⁺ = 280.1122.

4.3.10. *N*-Butyl-2-((6-methoxybenzo[d]thiazol-2-yl)amino)acetamide (**SN10**)

The compound was prepared with reference to compound **SN1** using intermediate **3b** (0.60 mmol, 1.0 equiv) and *n*-butylamine (0.72 mmol, 1.2 equiv) as raw material. The pure product was collected to give white solid **SN10** (91.4 mg, yield: 51.9%). ¹H NMR (400 MHz, DMSO- d_6) δ 8.00 (t, J = 5.8 Hz, 1H), 7.94 (t, J = 5.8 Hz, 1H), 7.35–7.23 (m, 2H), 6.82 (dd, J = 8.7, 2.6 Hz, 1H), 3.94 (d, J = 5.7 Hz, 2H), 3.08 (q, J = 6.5 Hz, 2H), 1.47–1.34 (m, 2H), 1.32–1.16 (m, 2H), 0.85 (t, J = 7.3 Hz, 3H). ¹³C NMR (101 MHz, DMSO- d_6) δ 169.04, 165.10, 154.88, 146.75, 132.16, 118.90, 113.39, 106.00, 55.99, 47.10, 38.65, 31.67, 19.94, 14.12. HRMS (ESI) of compound **SN10**: calcd for $C_{14}H_{19}N_3O_2S$ [M + H]⁺ = 292.1125, found [M + H]⁺ = 292.1118.

4.3.11. 2-((6-Methoxybenzo[d]thiazol-2-yl)amino)-*N*-pentylacetamide (**SN11**)

The compound was prepared with reference to compound **SN1** using intermediate **3b** (0.60 mmol, 1.0 equiv) and *n*-amylamine (0.72 mmol, 1.2 equiv) as raw material. The pure product was collected to give white solid **SN11** (95.9 mg, yield: 52.0%). ¹H NMR (400 MHz, DMSO- d_6) δ 7.97 (dt, J = 26.8, 6.0 Hz, 2H), 7.36–7.21 (m, 2H), 6.87–6.78 (m, 1H), 3.94 (d, J = 5.6 Hz, 2H), 3.73 (s, J = 2.4 Hz, 3H), 3.07 (q, J = 6.8 Hz, 2H), 1.40 (p, J = 7.2 Hz, 2H), 1.31–1.18 (m, 4H), 0.90–0.78 (m, 3H). ¹³C NMR (101 MHz, DMSO- d_6) δ 169.03, 165.09, 154.88, 146.75, 132.15, 118.90, 113.38, 106.00, 55.99, 47.10, 38.94, 29.24, 28.99, 22.31, 14.36. HRMS (ESI) of compound **SN11**: calcd for $C_{15}H_{21}N_3O_2S$ [M + H]⁺ = 308.1428, found [M + H]⁺ = 308.1440.

4.3.12. *N*-Hexyl-2-((6-methoxybenzo[d]thiazol-2-yl)amino)acetamide (**SN12**)

The compound was prepared with reference to compound **SN1** using intermediate **3b** (0.60 mmol, 1.0 equiv) and *n*-hexylamine (0.72 mmol, 1.2 equiv) as raw material. The pure product was collected to give white solid **SN12** (98.6 mg, yield: 51.5%). ¹H NMR (400 MHz, DMSO- d_6) δ 7.98 (dt, J = 29.1, 5.9 Hz, 2H), 7.28 (d, J = 9.5 Hz, 2H), 6.87–6.74 (m, 1H), 3.96 (d, J = 5.5 Hz, 2H), 3.73 (s, 3H), 3.08 (q, J = 6.7 Hz, 2H), 1.39 (t, J = 7.1 Hz, 2H), 1.22 (d, J = 8.2 Hz, 6H), 0.88–0.76 (m, 3H). ¹³C NMR (101 MHz, DMSO- d_6) δ 169.08, 165.11, 154.90, 146.76, 132.17, 118.91, 113.35, 105.94, 55.95, 47.14, 39.01, 31.48, 29.53, 26.50,

22.53, 14.33. HRMS (ESI) of compound **SN12**: calcd for $C_{16}H_{23}N_3O_2S$ [M + H]⁺ = 322.1584, found [M + H]⁺ = 322.1594.

4.3.13. *N*-Heptyl-2-((6-methoxybenzo[d]thiazol-2-yl)amino)acetamide (**SN13**)

The compound was prepared with reference to compound **SN1** using intermediate **3b** (0.60 mmol, 1.0 equiv) and *n*-heptanamine (0.72 mmol, 1.2 equiv) as raw material. The pure product was collected to give white solid **SN13** (111.0 mg, yield: 55.2%). ¹H NMR (400 MHz, DMSO- d_6) δ 7.97 (dt, J = 30.9, 5.6 Hz, 2H), 7.44–7.10 (m, 2H), 6.82 (dd, J = 8.7, 2.9 Hz, 1H), 3.93 (d, J = 5.6 Hz, 2H), 3.73 (d, J = 3.6 Hz, 3H), 3.07 (q, J = 6.5 Hz, 2H), 1.38 (q, J = 6.6 Hz, 2H), 1.30–1.09 (m, 8H), 0.83 (t, J = 6.8 Hz, 3H). ¹³C NMR (101 MHz, DMSO- d_6) δ 169.03, 165.08, 154.88, 146.75, 132.16, 118.90, 113.37, 105.98, 55.98, 47.12, 38.96, 31.71, 29.56, 28.91, 26.76, 22.52, 14.40. HRMS (ESI) of compound **SN13**: calcd for $C_{17}H_{25}N_3O_2S$ [M + H]⁺ = 336.1741, found [M + H]⁺ = 336.1747.

4.3.14. 2-((6-Methoxybenzo[d]thiazol-2-yl)amino)-*N*-octylacetamide (**SN14**)

The compound was prepared with reference to compound **SN1** using intermediate **3b** (0.60 mmol, 1.0 equiv) and *n*-octylamine (0.72 mmol, 1.2 equiv) as raw material. The pure product was collected to give white solid **SN14** (106.5 mg, yield: 50.8%). ¹H NMR (400 MHz, DMSO- d_6) δ 7.97 (dd, J = 34.9, 6.0 Hz, 2H), 7.35–7.21 (m, 2H), 6.86–6.75 (m, 1H), 3.94 (s, 2H), 3.74 (d, J = 1.9 Hz, 3H), 3.07 (q, J = 6.7 Hz, 2H), 1.38 (q, J = 7.1 Hz, 2H), 1.23 (d, J = 12.2 Hz, 10H), 0.90–0.78 (m, 3H). ¹³C NMR (101 MHz, DMSO- d_6) δ 169.01, 165.10, 154.89, 145.83, 132.12, 118.88, 113.38, 106.00, 55.99, 47.12, 38.96, 31.71, 29.56, 29.21, 29.13, 26.81, 22.56, 14.40. HRMS (ESI) of compound **SN14**: calcd for $C_{17}H_{25}N_3OS$ [M + H]⁺ = 350.1897, found [M + H]⁺ = 350.1911.

4.3.15. 2-((6-Chlorobenzo[d]thiazol-2-yl)amino)-*N*-ethylacetamide (**SN15**)

The compound was prepared with reference to compound **SN1** using intermediate **3c** (0.60 mmol, 1.0 equiv) and ethylamine (0.72 mmol, 1.2 equiv) as raw material. The pure product was collected to give white solid **SN15** (72.3 mg, yield: 44.7%). ¹H NMR (400 MHz, DMSO- d_6) δ 8.35 (t, J = 5.7 Hz, 1H), 8.02 (t, J = 5.6 Hz, 1H), 7.80 (d, J = 2.2 Hz, 1H), 7.34 (d, J = 8.6 Hz, 1H), 7.23 (dd, J = 8.6, 2.2 Hz, 1H), 3.98 (d, J = 5.6 Hz, 2H), 3.19–3.02 (m, 2H), 1.02 (t, J = 7.2 Hz, 3H). ¹³C NMR (101 MHz, DMSO- d_6) δ 168.56, 167.34, 151.60, 132.85, 126.08, 125.23, 121.11, 119.43, 47.03, 33.91, 15.17. HRMS (ESI) of compound **SN15**: calcd for $C_{11}H_{12}ClN_3OS$ [M + H]⁺ = 270.0463, found [M + H]⁺ = 270.0456.

4.3.16. 2-((6-Chlorobenzo[d]thiazol-2-yl)amino)-*N*-propylacetamide (**SN16**)

The compound was prepared with reference to compound **SN1** using intermediate **3c** (0.60 mmol, 1.0 equiv) and *n*-propylamine (0.72 mmol, 1.2 equiv) as raw material. The pure product was collected to give white solid **SN16** (97.9 mg, yield: 57.5%). ¹H NMR (400 MHz, DMSO- d_6) δ 8.37 (t, J = 5.4 Hz, 1H), 8.01 (t, J = 5.5 Hz, 1H), 7.80 (t, J = 1.8 Hz, 1H), 7.34 (dd, J = 8.6, 1.2 Hz, 1H), 7.23 (dt, J = 8.3, 1.8 Hz, 1H), 4.00 (d, J = 5.6 Hz, 2H), 3.09–3.01 (m, 2H), 1.42 (h, J = 7.2 Hz, 2H), 0.84 (td, J = 7.5, 1.3 Hz, 3H). ¹³C NMR (101 MHz, DMSO- d_6) δ 168.73,

167.31, 151.62, 132.87, 126.07, 125.22, 121.11, 119.40, 47.04, 40.81, 22.81, 11.80. HRMS (ESI) of compound **SN16**: calcd for $C_{12}H_{14}ClN_3OS$ $[M + H]^+$ = 284.0619, found $[M + H]^+$ = 284.0612.

4.3.17. *N*-Butyl-2-((6-chlorobenzothiazol-2-yl)amino)acetamide (**SN17**)

The compound was prepared with reference to compound **SN1** using intermediate **3c** (0.60 mmol, 1.0 equiv) and *n*-butylamine (0.72 mmol, 1.2 equiv) as raw material. The pure product was collected to give white solid **SN17** (83.6 mg, yield: 46.9%). 1H NMR (400 MHz, DMSO- d_6) δ 8.35 (s, 1H), 7.89 (d, J = 73.9 Hz, 2H), 7.28 (d, J = 41.1 Hz, 2H), 3.98 (s, 2H), 3.08 (s, 2H), 1.33 (d, J = 44.1 Hz, 4H), 0.85 (s, 3H). ^{13}C NMR (101 MHz, DMSO- d_6) δ 168.67, 167.30, 151.56, 132.84, 126.05, 125.26, 121.09, 119.38, 47.03, 38.66, 31.62, 19.92, 14.11. HRMS (ESI) of compound **SN17**: calcd for $C_{13}H_{16}ClN_3OS$ $[M + H]^+$ = 298.0776, found $[M + H]^+$ = 298.0790.

4.3.18. 2-((6-Chlorobenzothiazol-2-yl)amino)-*N*-pentylacetamide (**SN18**)

The compound was prepared with reference to compound **SN1** using intermediate **3c** (0.60 mmol, 1.0 equiv) and *n*-amylamine (0.72 mmol, 1.2 equiv) as raw material. The pure product was collected to give white solid **SN18** (97.4 mg, yield: 49.0%). 1H NMR (400 MHz, DMSO- d_6) δ 8.36 (t, J = 5.7 Hz, 1H), 7.98 (t, J = 5.7 Hz, 1H), 7.80 (d, J = 2.2 Hz, 1H), 7.34 (d, J = 8.5 Hz, 1H), 7.23 (dd, J = 8.6, 2.3 Hz, 1H), 3.98 (d, J = 5.7 Hz, 2H), 3.07 (q, J = 6.6 Hz, 2H), 1.40 (p, J = 7.0 Hz, 2H), 1.29–1.19 (m, 4H), 0.83 (t, J = 6.8 Hz, 3H). ^{13}C NMR (101 MHz, DMSO- d_6) δ 168.68, 167.30, 151.61, 132.86, 126.06, 125.23, 121.09, 119.40, 47.05, 38.96, 29.22, 28.99, 22.30, 14.36. HRMS (ESI) of compound **SN18**: calcd for $C_{14}H_{18}ClN_3OS$ $[M + H]^+$ = 312.0932, found $[M + H]^+$ = 312.0922.

4.3.19. 2-((6-Chlorobenzothiazol-2-yl)amino)-*N*-hexylacetamide (**SN19**)

The compound was prepared with reference to compound **SN1** using intermediate **3c** (0.60 mmol, 1.0 equiv) and *n*-hexylamine (0.72 mmol, 1.2 equiv) as raw material. The pure product was collected to give white solid **SN19** (94.0 mg, yield: 48.1%). 1H NMR (400 MHz, DMSO- d_6) δ 8.36 (t, J = 5.7 Hz, 1H), 7.98 (t, J = 5.7 Hz, 1H), 7.80 (d, J = 2.2 Hz, 1H), 7.33 (d, J = 8.5 Hz, 1H), 7.23 (dd, J = 8.5, 2.2 Hz, 1H), 3.98 (d, J = 5.6 Hz, 2H), 3.07 (q, J = 6.6 Hz, 2H), 1.38 (q, J = 6.9 Hz, 2H), 1.28–1.18 (m, 6H), 0.87–0.79 (m, 3H). ^{13}C NMR (101 MHz, DMSO- d_6) δ 168.68, 167.28, 151.59, 126.06, 125.22, 121.10, 119.40, 47.04, 39.00, 31.45, 29.50, 26.47, 22.51, 14.37. HRMS (ESI) of compound **SN19**: calcd for $C_{15}H_{20}ClN_3OS$ $[M + H]^+$ = 326.1089, found $[M + H]^+$ = 326.1082.

4.3.20. 2-((6-Chlorobenzothiazol-2-yl)amino)-*N*-heptylacetamide (**SN20**)

The compound was prepared with reference to compound **SN1** using intermediate **3c** (0.60 mmol, 1.0 equiv) and *n*-heptanamine (0.72 mmol, 1.2 equiv) as raw material. The pure product was collected to give white solid **SN20** (97.1 mg, yield: 47.6%). 1H NMR (400 MHz, methanol- d_4) δ 7.67 (d, J = 2.2 Hz, 1H), 7.40 (d, J = 8.5 Hz, 1H), 7.26 (dd, J = 8.6, 2.2 Hz, 1H), 4.08 (s, 2H), 3.21 (q, J = 5.7, 4.4 Hz, 2H), 1.49 (q, J = 7.1 Hz, 2H), 1.27 (qd, J = 7.6, 3.5 Hz, 8H), 0.88 (t, J = 6.9 Hz, 3H). ^{13}C NMR (101 MHz, Methanol- d_4) δ 169.11, 166.86, 149.96, 131.37,

125.64, 125.06, 119.54, 118.26, 45.97, 38.26, 30.77, 28.27, 27.96, 25.72, 21.48, 12.39. HRMS (ESI) of compound **SN20**: calcd for $C_{16}H_{22}ClN_3OS$ $[M + H]^+$ = 340.1245, found $[M + H]^+$ = 340.1238.

4.3.21. 2-((6-Nitrobenzothiazol-2-yl)amino)-*N*-propylacetamide (**SN21**)

The compound was prepared with reference to compound **SN1** using intermediate **3d** (0.60 mmol, 1.0 equiv) and *n*-propylamine (0.72 mmol, 1.2 equiv) as raw material. The pure product was collected to give yellow solid **SN21** (76.3 mg, yield: 43.2%). 1H NMR (400 MHz, DMSO- d_6) δ 8.97 (d, J = 5.7 Hz, 1H), 8.72 (q, J = 2.0 Hz, 1H), 8.10 (ddd, J = 8.0, 5.0, 3.1 Hz, 2H), 7.46 (ddd, J = 9.0, 3.4, 1.5 Hz, 1H), 4.08 (d, J = 5.5 Hz, 2H), 3.06 (q, J = 6.5 Hz, 2H), 1.42 (dt, J = 11.4, 4.3 Hz, 2H), 0.85 (tt, J = 7.5, 2.4 Hz, 3H). ^{13}C NMR (101 MHz, DMSO- d_6) δ 171.53, 168.33, 158.25, 141.40, 131.87, 122.51, 118.21, 117.80, 47.12, 40.88, 22.73, 11.75. HRMS (ESI) of compound **SN21**: calcd for $C_{12}H_{14}N_4O_3S$ $[M + H]^+$ = 295.0860, found $[M + H]^+$ = 295.0866.

4.3.22. *N*-Butyl-2-((6-nitrobenzothiazol-2-yl)amino)acetamide (**SN22**)

The compound was prepared with reference to compound **SN1** using intermediate **3d** (0.60 mmol, 1.0 equiv) and *n*-butylamine (0.72 mmol, 1.2 equiv) as raw material. The pure product was collected to give yellow solid **SN22** (64.0 mg, yield: 34.6%). 1H NMR (400 MHz, DMSO- d_6) δ 8.96 (t, J = 5.6 Hz, 1H), 8.72 (d, J = 2.5 Hz, 1H), 8.15–8.01 (m, 2H), 7.45 (d, J = 8.9 Hz, 1H), 4.08 (d, J = 5.6 Hz, 2H), 3.09 (q, J = 6.5 Hz, 2H), 1.44–1.34 (m, 2H), 1.32–1.24 (m, 2H), 0.86 (t, J = 7.3 Hz, 3H). ^{13}C NMR (101 MHz, DMSO- d_6) δ 168.22, 158.34, 141.30, 131.95, 122.46, 118.26, 117.71, 47.13, 38.71, 31.62, 19.94, 14.12. HRMS (ESI) of compound **SN22**: calcd for $C_{13}H_{16}N_4O_3S$ $[M + H]^+$ = 309.1016, found $[M + H]^+$ = 309.1027.

4.3.23. 2-((6-Nitrobenzothiazol-2-yl)amino)-*N*-pentylacetamide (**SN23**)

The compound was prepared with reference to compound **SN1** using intermediate **3d** (0.60 mmol, 1.0 equiv) and *n*-amylamine (0.72 mmol, 1.2 equiv) as raw material. The pure product was collected to give yellow solid **SN23** (83.0 mg, yield: 42.9%). 1H NMR (400 MHz, DMSO- d_6) δ 9.12–8.92 (m, 1H), 8.70 (d, J = 13.8 Hz, 1H), 8.10 (q, J = 11.0, 9.7 Hz, 2H), 7.45 (dd, J = 15.9, 8.5 Hz, 1H), 4.06 (d, J = 13.8 Hz, 2H), 3.08 (dd, J = 14.1, 7.6 Hz, 2H), 1.46–1.33 (m, 2H), 1.32–1.15 (m, 4H), 0.83 (dd, J = 14.4, 7.2 Hz, 3H). ^{13}C NMR (101 MHz, DMSO- d_6) δ 171.50, 168.20, 158.31, 141.34, 131.93, 122.48, 118.28, 117.75, 47.12, 39.01, 29.18, 28.98, 22.28, 14.36. HRMS (ESI) of compound **SN23**: calcd for $C_{14}H_{18}N_4O_3S$ $[M + H]^+$ = 323.1173, found $[M + H]^+$ = 323.1167.

4.3.24. *N*-Hexyl-2-((6-nitrobenzothiazol-2-yl)amino)acetamide (**SN24**)

The compound was prepared with reference to compound **SN1** using intermediate **3d** (0.60 mmol, 1.0 equiv) and *n*-hexylamine (0.72 mmol, 1.2 equiv) as raw material. The pure product was collected to give yellow solid **SN24** (82.2 mg, yield: 40.7%). 1H NMR (400 MHz, DMSO- d_6) δ 8.96 (s, 1H), 8.71 (d, J = 2.5 Hz, 1H), 8.15–8.01 (m, 2H), 7.45 (d, J = 8.9 Hz, 1H), 4.07 (s, 2H), 3.08 (q, J = 6.6 Hz, 2H), 1.40 (p, J = 7.1, 6.4 Hz, 2H), 1.23 (s, 6H), 0.83 (d, J = 6.8 Hz, 3H). ^{13}C NMR (101 MHz, DMSO- d_6)

δ 171.55, 168.43, 158.32, 141.24, 131.84, 122.51, 118.16, 117.69, 47.28, 39.05, 31.39, 29.39, 26.41, 22.46, 14.32. HRMS (ESI) of compound **SN24**: calcd for $C_{15}H_{20}N_4O_3S$ $[M + H]^+$ = 337.1329, found $[M + H]^+$ = 337.1321.

4.3.25. *N*-Heptyl-2-((6-nitrobenzo[d]thiazol-2-yl)amino)acetamide (**SN25**)

The compound was prepared with reference to compound **SN1** using intermediate **3d** (0.60 mmol, 1.0 equiv) and *n*-heptanamine (0.72 mmol, 1.2 equiv) as raw material. The pure product was collected to give yellow solid **SN25** (89.6 mg, yield: 42.6%). 1H NMR (400 MHz, DMSO- d_6) δ 8.96 (d, J = 6.5 Hz, 1H), 8.70 (d, J = 13.5 Hz, 1H), 8.14–7.96 (m, 2H), 7.49–7.36 (m, 1H), 4.07 (d, J = 5.6 Hz, 2H), 3.08 (q, J = 6.9 Hz, 2H), 1.39 (q, J = 7.2 Hz, 2H), 1.21 (d, J = 10.5 Hz, 8H), 0.83 (t, J = 7.0 Hz, 3H). ^{13}C NMR (101 MHz, DMSO- d_6) δ 168.17, 158.32, 154.14, 141.33, 131.95, 122.44, 118.28, 117.73, 47.16, 39.02, 31.71, 29.52, 28.89, 26.75, 22.51, 14.40. HRMS (ESI) of compound **SN25**: calcd for $C_{16}H_{22}N_4O_3S$ $[M + H]^+$ = 351.1486, found $[M + H]^+$ = 351.1477.

4.3.26. 2-((6-Nitrobenzo[d]thiazol-2-yl)amino)-*N*-octylacetamide (**SN26**)

The compound was prepared with reference to compound **SN1** using intermediate **3d** (0.60 mmol, 1.0 equiv) and *n*-octylamine (0.72 mmol, 1.2 equiv) as raw material. The pure product was collected to give yellow solid **SN26** (88.4 mg, yield: 40.4%). 1H NMR (400 MHz, DMSO- d_6) δ 8.95 (t, J = 5.7 Hz, 1H), 8.70 (d, J = 2.5 Hz, 1H), 8.13–8.01 (m, 2H), 7.45 (d, J = 8.9 Hz, 1H), 4.06 (d, J = 5.5 Hz, 2H), 3.07 (q, J = 6.5 Hz, 2H), 1.38 (q, J = 7.0 Hz, 2H), 1.25–1.16 (m, 10H), 0.82 (t, J = 6.7 Hz, 3H). ^{13}C NMR (101 MHz, DMSO- d_6) δ 171.45, 168.17, 158.32, 141.33, 131.95, 122.44, 118.28, 117.73, 47.15, 39.02, 31.69, 29.51, 29.19, 29.13, 26.80, 22.55, 14.39. HRMS (ESI) of compound **SN26**: calcd for $C_{17}H_{24}N_4O_3S$ $[M + H]^+$ = 365.1642, found $[M + H]^+$ = 365.1645.

4.4. General procedure for the synthesis of target compounds **SN27** to **SN39**

4.4.1. *N*-Hexyl-2-(phenylamino)acetamide (**SN27**)

The compound was synthesized by one-pot method: intermediate **4a** (0.60 mmol, 1.0 equiv) was dissolved in acetonitrile and after addition of aniline (0.72 mmol, 1.2 equiv), KI (0.06 mmol, 0.1 equiv) and K_2CO_3 (0.90 mmol, 1.5 equiv), the mixture was stirred at 60 °C for 6 h. The reaction was terminated by TLC detection. The reaction solution was extracted with EtOAc (30 mL \times 3), washed with saturated NH_4Cl solution and saturated NaCl solution, respectively, until the neutral pH. The combined organic phases were sufficiently dried with $MgSO_4$ and the solvent was removed in vacuum. The crude product was purified by flash chromatography (petroleum/EtOAc, 2:1). The pure product was collected to give brown oily liquid **SN27** (115.4 mg, yield: 82.1%). 1H NMR (400 MHz, chloroform- d) δ 7.18 (t, J = 7.8 Hz, 2H), 6.84 (t, J = 6.0 Hz, 1H), 6.78 (t, J = 7.3 Hz, 1H), 6.60 (d, J = 8.0 Hz, 2H), 3.74 (s, 2H), 3.24 (q, J = 6.8 Hz, 2H), 1.43 (p, J = 7.1 Hz, 2H), 1.22 (d, J = 2.6 Hz, 6H), 0.84 (t, J = 6.7 Hz, 3H). ^{13}C NMR (101 MHz, $CDCl_3$) δ 170.59, 147.35, 129.40 (2C), 118.91, 113.18 (2C), 48.84, 39.25, 31.42, 29.51, 26.50, 22.52, 13.99. HRMS (ESI) of compound **SN27**: calcd for $C_{14}H_{22}N_2O$ $[M-H]^+$ = 233.1659, found $[M-H]^+$ = 233.1651.

4.4.2. *N*-Heptyl-2-(phenylamino)acetamide (**SN28**)

The compound was prepared with reference to compound **SN27** using intermediate **4b** (0.60 mmol, 1.0 equiv) and aniline (0.72 mmol, 1.2 equiv) as raw material. The pure product was collected to give brown oily liquid **SN28** (135.3 mg, yield: 90.8%). 1H NMR (400 MHz, DMSO- d_6) δ 7.80 (t, J = 5.7 Hz, 1H), 7.07 (t, J = 7.7 Hz, 2H), 6.63–6.47 (m, 3H), 5.89 (t, J = 5.8 Hz, 1H), 3.58 (d, J = 5.7 Hz, 2H), 3.06 (q, J = 6.6 Hz, 2H), 1.38 (q, J = 6.7 Hz, 2H), 1.23 (d, J = 12.8 Hz, 8H), 0.85 (t, J = 6.8 Hz, 3H). ^{13}C NMR (101 MHz, DMSO- d_6) δ 170.39, 148.85, 129.25 (2C), 116.84, 112.77 (2C), 47.47, 38.81, 31.70, 29.59, 28.87, 26.73, 22.50, 14.40. HRMS (ESI) of compound **SN28**: calcd for $C_{15}H_{24}N_2O$ $[M-H]^+$ = 247.1815, found $[M-H]^+$ = 247.1810.

4.4.3. *N*-Octyl-2-(phenylamino)acetamide (**SN29**)

The compound was prepared with reference to compound **SN27** using intermediate **4c** (0.60 mmol, 1.0 equiv) and aniline (0.72 mmol, 1.2 equiv) as raw material. The pure product was collected to give brown oily liquid **SN29** (120.1 mg, yield: 76.3%). 1H NMR (400 MHz, DMSO- d_6) δ 7.80 (t, J = 5.7 Hz, 1H), 7.07 (t, J = 7.6 Hz, 2H), 6.61–6.46 (m, 3H), 5.89 (s, 1H), 3.58 (d, J = 3.8 Hz, 2H), 3.06 (q, J = 6.5 Hz, 2H), 1.37 (q, J = 6.6 Hz, 2H), 1.26–1.19 (m, 10H), 0.86 (d, J = 6.3 Hz, 3H). ^{13}C NMR (101 MHz, DMSO- d_6) δ 170.39, 148.85, 129.25 (2C), 116.84, 112.76 (2C), 47.47, 38.81, 31.69, 29.58, 29.18, 29.12, 26.77, 22.56, 14.41. HRMS (ESI) of compound **SN29**: calcd for $C_{16}H_{26}N_2O$ $[M + H]^+$ = 263.2118, found $[M + H]^+$ = 263.2108.

4.4.4. 2-((3-Chlorophenyl)amino)-*N*-hexylacetamide (**SN30**)

The compound was prepared with reference to compound **SN27** using intermediate **4a** (0.60 mmol, 1.0 equiv) and 3-chloroaniline (0.72 mmol, 1.2 equiv) as raw material. The pure product was collected to give brown oily liquid **SN30** (150.4 mg, yield: 93.3%). 1H NMR (400 MHz, DMSO- d_6) δ 7.87 (t, J = 5.8 Hz, 1H), 7.06 (t, J = 8.0 Hz, 1H), 6.62–6.44 (m, 3H), 6.27 (t, J = 6.1 Hz, 1H), 3.61 (d, J = 6.0 Hz, 2H), 3.06 (q, J = 6.6 Hz, 2H), 1.40–1.33 (m, 2H), 1.23 (dd, J = 11.4, 4.4 Hz, 6H), 0.84 (t, J = 6.9 Hz, 3H). ^{13}C NMR (101 MHz, DMSO- d_6) δ 169.91, 150.39, 134.01, 130.72, 116.07, 111.88, 111.50, 46.94, 38.85, 31.47, 29.54, 26.45, 22.51, 14.37. HRMS (ESI) of compound **SN30**: calcd for $C_{14}H_{21}ClN_2O$ $[M-H]^+$ = 267.1269, found $[M-H]^+$ = 267.1263.

4.4.5. 2-((3-Chlorophenyl)amino)-*N*-heptylacetamide (**SN31**)

The compound was prepared with reference to compound **SN27** using intermediate **4b** (0.60 mmol, 1.0 equiv) and 3-chloroaniline (0.72 mmol, 1.2 equiv) as raw material. The pure product was collected to give brown oily liquid **SN31** (131.5 mg, yield: 77.5%). 1H NMR (400 MHz, chloroform- d) δ 7.11 (t, J = 8.1 Hz, 1H), 6.78 (dd, J = 7.8, 1.9 Hz, 1H), 6.61 (t, J = 2.1 Hz, 1H), 6.50 (dt, J = 8.2, 4.6 Hz, 2H), 3.77 (s, 2H), 3.27 (q, J = 6.7 Hz, 2H), 1.46 (p, J = 7.2 Hz, 2H), 1.25 (d, J = 6.7 Hz, 8H), 0.86 (t, J = 6.7 Hz, 3H). ^{13}C NMR (101 MHz, $CDCl_3$) δ 169.54, 148.16, 135.27, 130.45, 119.17, 113.29, 111.52, 48.55, 39.34, 31.69, 29.53, 28.88, 26.77, 22.54, 14.03. HRMS (ESI) of compound **SN31**: calcd for $C_{15}H_{23}ClN_2O$ $[M-H]^+$ = 281.1426, found $[M-H]^+$ = 281.1418.

4.4.6. 2-((3-Chlorophenyl)amino)-*N*-octylacetamide (**SN32**)

The compound was prepared with reference to compound **SN27** using intermediate **4c** (0.60 mmol, 1.0 equiv) and 3-chloroaniline

(0.72 mmol, 1.2 equiv) as raw material. The pure product was collected to give brown oily liquid **SN32** (117.0 mg, yield: 65.7%). ^1H NMR (400 MHz, chloroform-*d*) δ 7.15–7.00 (m, 1H), 6.74 (d, $J = 7.3$ Hz, 1H), 6.67–6.51 (m, 2H), 6.50–6.42 (m, 1H), 3.78–3.65 (m, 2H), 3.25 (q, $J = 6.9$, 6.2 Hz, 2H), 1.50–1.36 (m, 2H), 1.22 (s, 10H), 0.89–0.77 (m, 3H). ^{13}C NMR (101 MHz, CDCl_3) δ 169.80, 148.37, 135.19, 130.43, 118.89, 113.13, 111.37, 48.42, 39.34, 31.75, 29.53, 29.21, 29.17, 26.84, 22.63, 14.08. HRMS (ESI) of compound **SN32**: calcd for $\text{C}_{16}\text{H}_{25}\text{ClN}_2\text{O}$ $[\text{M}-\text{H}]^+ = 295.1582$, found $[\text{M}-\text{H}]^+ = 295.1575$.

4.4.7. *N*-Hexyl-2-((4-methoxyphenyl)amino)acetamide (**SN33**)

The compound was prepared with reference to compound **SN27** using intermediate **4a** (0.60 mmol, 1.0 equiv) and *p*-anisidine (0.72 mmol, 1.2 equiv) as raw material. The pure product was collected to give brown oily liquid **SN33** (101.0 mg, yield: 63.7%). ^1H NMR (400 MHz, chloroform-*d*) δ 6.84 (d, $J = 6.7$ Hz, 1H), 6.80–6.74 (m, 2H), 6.55 (dd, $J = 8.9$, 2.2 Hz, 2H), 3.73 (d, $J = 2.0$ Hz, 3H), 3.70 (d, $J = 2.0$ Hz, 2H), 3.24 (q, $J = 6.7$, 6.3 Hz, 2H), 1.48–1.39 (m, 2H), 1.22 (h, $J = 2.5$, 2.1 Hz, 6H), 0.83 (td, $J = 6.9$, 2.3 Hz, 3H). ^{13}C NMR (101 MHz, CDCl_3) δ 170.71, 153.11, 141.31, 114.93 (2C), 114.37 (2C), 55.72, 49.72, 39.16, 31.42, 29.52, 26.49, 22.52, 13.97. HRMS (ESI) of compound **SN33**: calcd for $\text{C}_{15}\text{H}_{24}\text{N}_2\text{O}_2$ $[\text{M}-\text{H}]^+ = 263.1765$, found $[\text{M}-\text{H}]^+ = 263.1760$.

4.4.8. *N*-Heptyl-2-((4-methoxyphenyl)amino)acetamide (**SN34**)

The compound was prepared with reference to compound **SN27** using intermediate **4b** (0.60 mmol, 1.0 equiv) and *p*-anisidine (0.72 mmol, 1.2 equiv) as raw material. The pure product was collected to give brown oily liquid **SN34** (120.0 mg, yield: 71.8%). ^1H NMR (400 MHz, $\text{DMSO}-d_6$) δ 7.76 (t, $J = 5.9$ Hz, 1H), 6.75–6.69 (m, 2H), 6.51–6.46 (m, 2H), 5.54 (t, $J = 5.9$ Hz, 1H), 3.63 (s, 3H), 3.53 (d, $J = 5.7$ Hz, 2H), 3.06 (q, $J = 6.6$ Hz, 2H), 1.36 (p, $J = 7.1$ Hz, 2H), 1.26–1.14 (m, 8H), 0.85 (t, $J = 6.9$ Hz, 3H). ^{13}C NMR (101 MHz, $\text{DMSO}-d_6$) δ 170.66, 151.68, 143.01, 114.95 (2C), 113.81 (2C), 55.73, 48.41, 38.77, 31.72, 29.60, 28.90, 26.73, 22.51, 14.40. HRMS (ESI) of compound **SN34**: calcd for $\text{C}_{16}\text{H}_{26}\text{N}_2\text{O}_2$ $[\text{M}-\text{H}]^+ = 277.1921$, found $[\text{M}-\text{H}]^+ = 277.1913$.

4.4.9. *N*-Hexyl-2-((2-methoxyphenyl)amino)acetamide (**SN35**)

The compound was prepared with reference to compound **SN27** using intermediate **4a** (0.60 mmol, 1.0 equiv) and *o*-anisidine (0.72 mmol, 1.2 equiv) as raw material. The pure product was collected to give brown oily liquid **SN35** (136.8 mg, yield: 86.2%). ^1H NMR (400 MHz, $\text{DMSO}-d_6$) δ 7.86 (t, $J = 5.8$ Hz, 1H), 6.85–6.70 (m, 2H), 6.66–6.52 (m, 1H), 6.34 (d, $J = 7.7$ Hz, 1H), 5.26 (s, 1H), 3.79 (s, 3H), 3.62 (s, 2H), 3.35 (s, 2H), 3.07 (q, $J = 6.6$ Hz, 2H), 1.37 (t, $J = 6.9$ Hz, 2H), 1.26–1.18 (m, 6H), 0.84 (t, $J = 6.7$ Hz, 3H). ^{13}C NMR (101 MHz, $\text{DMSO}-d_6$) δ 170.07, 146.97, 138.08, 121.42, 116.78, 110.18, 109.89, 55.73, 47.14, 38.88, 31.44, 29.52, 26.46, 22.52, 14.35. HRMS (ESI) of compound **SN35**: calcd for $\text{C}_{15}\text{H}_{24}\text{N}_2\text{O}_2$ $[\text{M}-\text{H}]^+ = 263.1765$, found $[\text{M}-\text{H}]^+ = 263.1759$.

4.4.10. *N*-Heptyl-2-((2-methoxyphenyl)amino)acetamide (**SN36**)

The compound was prepared with reference to compound **SN27** using intermediate **4b** (0.60 mmol, 1.0 equiv) and *o*-anisidine (0.72 mmol, 1.2 equiv) as raw material. The pure product was collected to give brown oily liquid **SN36** (141.0 mg, yield:

84.4%). ^1H NMR (400 MHz, chloroform-*d*) δ 6.82 (ddp, $J = 23.9$, 17.0, 8.7, 7.2 Hz, 4H), 6.56–6.46 (m, 1H), 3.88 (q, $J = 5.3$, 4.7 Hz, 3H), 3.79 (t, $J = 5.2$ Hz, 2H), 3.25 (p, $J = 5.2$ Hz, 2H), 1.53–1.36 (m, 2H), 1.28–1.19 (m, 8H), 0.86 (dq, $J = 10.3$, 5.2, 4.6 Hz, 3H). ^{13}C NMR (101 MHz, CDCl_3) δ 170.59, 146.94, 137.16, 121.37, 118.45, 110.67, 109.57, 55.45, 48.89, 39.16, 31.69, 29.55, 28.89, 26.77, 22.53, 14.04. HRMS (ESI) of compound **SN36**: calcd for $\text{C}_{16}\text{H}_{26}\text{N}_2\text{O}_2$ $[\text{M}-\text{H}]^+ = 277.1921$, found $[\text{M}-\text{H}]^+ = 277.1915$.

4.4.11. *N*-Hexyl-2-(thiazol-2-ylamino)acetamide (**SN37**)

The compound was prepared with reference to compound **SN27** using intermediate **4a** (0.60 mmol, 1.0 equiv) and 2-aminothiazole (0.72 mmol, 1.2 equiv) as raw material. The pure product was collected to give white solid **SN37** (50.0 mg, yield: 34.5%). ^1H NMR (400 MHz, $\text{DMSO}-d_6$) δ 7.87 (s, 1H), 7.71 (d, $J = 6.4$ Hz, 1H), 7.04–6.92 (m, 1H), 6.71–6.57 (m, 1H), 3.81 (dd, $J = 5.9$, 2.5 Hz, 2H), 3.05 (q, $J = 6.8$ Hz, 2H), 1.43–1.32 (m, 2H), 1.25 (d, $J = 11.5$ Hz, 6H), 0.93–0.77 (m, 3H). ^{13}C NMR (101 MHz, $\text{DMSO}-d_6$) δ 169.37, 169.30, 138.90, 107.27, 47.65, 38.93, 31.45, 29.52, 26.45, 22.52, 14.38. HRMS (ESI) of compound **SN37**: calcd for $\text{C}_{11}\text{H}_{19}\text{N}_3\text{OS}$ $[\text{M}-\text{H}]^+ = 240.1176$, found $[\text{M}-\text{H}]^+ = 240.1169$.

4.4.12. *N*-Heptyl-2-(thiazol-2-ylamino)acetamide (**SN38**)

The compound was prepared with reference to compound **SN27** using intermediate **4b** (0.60 mmol, 1.0 equiv) and 2-aminothiazole (0.72 mmol, 1.2 equiv) as raw material. The pure product was collected to give white solid **SN38** (71.0 mg, yield: 46.3%). ^1H NMR (400 MHz, $\text{DMSO}-d_6$) δ 7.86 (t, $J = 5.7$ Hz, 1H), 7.71 (t, $J = 5.9$ Hz, 1H), 6.99 (d, $J = 3.7$ Hz, 1H), 6.63 (d, $J = 3.7$ Hz, 1H), 3.81 (d, $J = 5.7$ Hz, 2H), 3.05 (q, $J = 6.6$ Hz, 2H), 1.38 (p, $J = 6.9$ Hz, 2H), 1.24 (d, $J = 3.4$ Hz, 8H), 0.86 (t, $J = 6.6$ Hz, 3H). ^{13}C NMR (101 MHz, DMSO) δ 169.36, 169.29, 138.90, 107.25, 47.65, 38.93, 31.71, 29.56, 28.88, 26.75, 22.51, 14.42. HRMS (ESI) of compound **SN38**: calcd for $\text{C}_{12}\text{H}_{21}\text{N}_3\text{OS}$ $[\text{M}-\text{H}]^+ = 254.1332$, found $[\text{M}-\text{H}]^+ = 254.1324$.

4.4.13. *N*-Octyl-2-(thiazol-2-ylamino)acetamide (**SN39**)

The compound was prepared with reference to compound **SN27** using intermediate **4c** (0.60 mmol, 1.0 equiv) and 2-aminothiazole (0.72 mmol, 1.2 equiv) as raw material. The pure product was collected to give white solid **SN39** (67.0 mg, yield: 41.4%). ^1H NMR (400 MHz, $\text{DMSO}-d_6$) δ 7.86 (t, $J = 5.6$ Hz, 1H), 7.70 (d, $J = 5.6$ Hz, 1H), 6.99 (d, $J = 4.0$ Hz, 1H), 6.63 (d, $J = 4.0$ Hz, 1H), 3.81 (t, $J = 5.1$ Hz, 2H), 3.05 (p, $J = 5.9$, 5.4 Hz, 2H), 1.42–1.33 (m, 2H), 1.23 (s, 10H), 0.85 (q, $J = 5.8$ Hz, 3H). ^{13}C NMR (101 MHz, $\text{DMSO}-d_6$) δ 169.35, 169.28, 138.89, 107.24, 47.65, 38.92, 31.70, 29.56, 29.19, 29.13, 26.80, 22.56, 14.42. HRMS (ESI) of compound **SN39**: calcd for $\text{C}_{13}\text{H}_{23}\text{N}_3\text{OS}$ $[\text{M}-\text{H}]^+ = 268.1489$, found $[\text{M}-\text{H}]^+ = 268.1482$.

4.5. General procedure for the synthesis of target compounds **SN40** to **SN41**

4.5.1. 2-(Hexylamino)-*N*-(6-methoxybenzo[d]thiazol-2-yl)acetamide (**SN40**)

6-Methoxybenzo[d]thiazol-2-amine (2.0 mmol, 1.0 equiv), Et_3N (3.0 mmol, 1.5 equiv) and DCM (5 mL) were stirred at 0 °C for 15 min, slowly dripping chloroacetyl chloride (2.2 mmol, 1.1 equiv), the temperature was gradually increased to room temperature, stirring the reaction for 2h. Extracted with dichloromethane

and saturated NaHCO_3 solution, dried and then evaporated to obtain the crude intermediate **5**. The intermediate **5** (2.0 mmol, 1.0 equiv), K_2CO_3 (3.0 mmol, 1.5 equiv) and acetonitrile (5 mL) were mixed in a 25 mL reaction flask, catalytic amount of KI was added, and refluxed at 80 °C. Add *n*-hexylamine and react for 4 h. After complete reaction, extract with ethyl acetate and wash with saturated NaCl solution. The organic phase was collected and dried, and the solvent was removed by spin distillation. The crude product was purified by flash chromatography (petroleum/EtOAc, 2:1). The pure product was collected to give light yellow solid **SN40** (151.5 mg, yield: 23.6%). ^1H NMR (400 MHz, $\text{DMSO-}d_6$) δ 7.63 (d, $J = 8.8$ Hz, 1H), 7.57 (d, $J = 2.6$ Hz, 1H), 7.03 (dd, $J = 8.8, 2.6$ Hz, 1H), 3.81 (s, 3H), 3.47 (s, 2H), 2.55 (t, $J = 7.1$ Hz, 2H), 1.42 (q, $J = 6.8$ Hz, 2H), 1.32–1.21 (m, 6H), 0.90–0.83 (m, 3H). ^{13}C NMR (101 MHz, $\text{DMSO-}d_6$) δ 171.11, 156.65, 156.02, 143.04, 133.27, 121.60, 115.42, 105.22, 58.73, 56.09, 31.57, 30.28, 27.15, 26.68, 22.47, 14.29. HRMS (ESI) of compound **SN40**: calcd for $\text{C}_{16}\text{H}_{23}\text{N}_3\text{O}_2\text{S}$ $[\text{M}-\text{H}]^+ = 320.1438$, found $[\text{M}-\text{H}]^+ = 320.1428$.

4.5.2. 2-(Heptylamino)-*N*-(6-methoxybenzo[d]thiazol-2-yl)acetamide (**SN41**)

The compound was prepared with reference to compound **SN40** using intermediate **5** (2 mmol, 1.0 equiv) and *n*-heptylamine (2.2 mmol, 1.1 equiv) as raw material. The pure product was collected to give light yellow solid **SN41** (187.0 mg, yield: 27.9%). ^1H NMR (400 MHz, $\text{DMSO-}d_6$) δ 7.62 (d, $J = 8.8$ Hz, 1H), 7.55 (d, $J = 2.6$ Hz, 1H), 7.02 (dd, $J = 8.8, 2.6$ Hz, 1H), 3.80 (s, 3H), 3.44 (s, 2H), 2.53 (t, $J = 7.3$ Hz, 2H), 1.41 (q, $J = 7.0$ Hz, 2H), 1.25 (q, $J = 5.2, 4.6$ Hz, 8H), 0.88–0.82 (m, 3H). ^{13}C NMR (101 MHz, $\text{DMSO-}d_6$) δ 168.60, 156.69, 156.11, 143.03, 133.26, 121.71, 115.45, 105.13, 56.07, 55.77, 43.71, 31.73, 28.93, 27.52, 26.65, 22.52, 14.38. HRMS (ESI) of compound **SN41**: calcd for $\text{C}_{17}\text{H}_{25}\text{N}_3\text{O}_2\text{S}$ $[\text{M}-\text{H}]^+ = 334.1594$, found $[\text{M}-\text{H}]^+ = 334.1586$.

4.6. General procedure for the synthesis of target compounds **SN42** to **SN45**

4.6.1. 2-((6-Methoxybenzo[d]thiazol-2-yl)amino)-*N*-phenethylacetamide (**SN42**)

The compound was prepared with reference to compound **SN12** using intermediate **3b** (1 mmol, 1.0 equiv) and phenylethylamine (1.1 mmol, 1.1 equiv) as raw material. The pure product was collected to give a white solid **SN42** (154.0 mg, yield: 45.1%). ^1H NMR (400 MHz, $\text{DMSO-}d_6$) δ 8.04 (q, $J = 6.3$ Hz, 2H), 7.35–7.15 (m, 7H), 6.83 (dd, $J = 8.8, 2.6$ Hz, 1H), 3.94 (d, $J = 5.7$ Hz, 2H), 3.74 (s, 3H), 3.32–3.28 (m, 2H), 2.72 (t, $J = 7.3$ Hz, 2H). ^{13}C NMR (101 MHz, $\text{DMSO-}d_6$) δ 169.21, 166.01, 154.90, 153.13, 146.66, 132.32, 129.12 (2C), 128.75 (2C), 126.52, 118.96, 113.41, 106.01, 56.00, 47.10, 35.60. HRMS (ESI) of compound **SN42**: calcd for $\text{C}_{18}\text{H}_{19}\text{N}_3\text{O}_2\text{S}$ $[\text{M}-\text{H}]^+ = 340.1125$, found $[\text{M}-\text{H}]^+ = 340.1115$.

4.6.2. *N*-(4-Ethylphenyl)-2-((6-methoxybenzo[d]thiazol-2-yl)amino)acetamide (**SN43**)

The compound was prepared with reference to compound **SN12** using intermediate **3b** (1 mmol, 1.0 equiv) and 4-ethylaniline (1.1 mmol, 1.1 equiv) as raw material. The pure product was collected to give white solid **SN43** (120.0 mg, yield: 35.2%). ^1H NMR (400 MHz, $\text{DMSO-}d_6$) δ 10.04 (s, 1H), 8.14 (t, $J = 5.9$ Hz, 1H), 7.51 (d, $J = 8.2$ Hz, 2H), 7.33

(d, $J = 2.6$ Hz, 1H), 7.28 (d, $J = 8.7$ Hz, 1H), 7.14 (d, $J = 8.2$ Hz, 2H), 6.82 (dd, $J = 8.8, 2.6$ Hz, 1H), 4.18 (d, $J = 5.8$ Hz, 2H), 3.74 (s, 3H), 2.59–2.52 (m, 2H), 1.15 (t, $J = 7.6$ Hz, 3H). ^{13}C NMR (101 MHz, $\text{DMSO-}d_6$) δ 168.04, 165.18, 154.91, 146.68, 139.11, 137.07, 132.18, 128.43 (2C), 119.63 (2C), 118.96, 113.43, 106.04, 56.00, 47.51, 28.05, 16.16. HRMS (ESI) of compound **SN43**: calcd for $\text{C}_{18}\text{H}_{19}\text{N}_3\text{O}_2\text{S}$ $[\text{M}-\text{H}]^+ = 340.1125$, found $[\text{M}-\text{H}]^+ = 340.1116$.

4.6.3. *N*-(Cyclohexylmethyl)-2-((6-methoxybenzo[d]thiazol-2-yl)amino)acetamide (**SN44**)

The compound was prepared with reference to compound **SN12** using intermediate **3b** (1 mmol, 1.0 equiv) and cyclohexane methylamine (1.1 mmol, 1.1 equiv) as raw material. The pure product was collected to give white solid **SN44** (148.5 mg, yield: 44.5%). ^1H NMR (400 MHz, $\text{DMSO-}d_6$) δ 7.96 (dt, $J = 35.9, 5.9$ Hz, 2H), 7.35–7.20 (m, 2H), 6.82 (dt, $J = 9.2, 4.6$ Hz, 1H), 3.95 (d, $J = 5.8$ Hz, 2H), 3.73 (d, $J = 6.0$ Hz, 3H), 2.94 (t, $J = 6.4$ Hz, 2H), 1.72–1.54 (m, 5H), 1.38 (ddt, $J = 15.1, 7.4, 3.7$ Hz, 1H), 1.19–1.02 (m, 3H), 0.85 (tt, $J = 11.5, 5.8$ Hz, 2H). ^{13}C NMR (101 MHz, $\text{DMSO-}d_6$) δ 169.13, 165.06, 154.89, 146.77, 132.17, 118.87, 113.39, 106.02, 56.01, 47.14, 45.22, 37.96, 30.77 (2C), 26.49, 25.89 (2C). HRMS (ESI) of compound **SN44**: calcd for $\text{C}_{17}\text{H}_{23}\text{N}_3\text{O}_2\text{S}$ $[\text{M}-\text{H}]^+ = 332.1438$, found $[\text{M}-\text{H}]^+ = 332.1430$.

4.6.4. 2-((6-Methoxybenzo[d]thiazol-2-yl)amino)-*N*-(2-morpholinoethyl)acetamide (**SN45**)

The compound was prepared with reference to compound **SN12** using intermediate **3b** (1 mmol, 1.0 equiv) and 2-morpholinoethan-1-amine (1.1 mmol, 1.1 equiv) as raw material. The pure product was collected to give white solid **SN45** (171.4 mg, yield: 48.9%). ^1H NMR (400 MHz, $\text{DMSO-}d_6$) δ 7.70 (d, $J = 8.8$ Hz, 1H), 7.62 (d, $J = 2.6$ Hz, 1H), 7.05 (dd, $J = 8.9, 2.6$ Hz, 1H), 4.67 (s, 2H), 3.82 (s, 3H), 3.63 (t, $J = 6.8$ Hz, 2H), 3.55 (t, $J = 4.6$ Hz, 4H), 2.53 (d, $J = 6.8$ Hz, 2H), 2.43 (t, $J = 4.6$ Hz, 4H). ^{13}C NMR (101 MHz, $\text{DMSO-}d_6$) δ 169.16, 156.76, 154.59, 143.20, 133.54, 121.83, 115.41, 105.60, 66.64 (2C), 56.10, 55.38, 53.55 (2C), 50.56, 36.28. HRMS (ESI) of compound **SN45**: calcd for $\text{C}_{16}\text{H}_{22}\text{N}_4\text{O}_3\text{S}$ $[\text{M}-\text{H}]^+ = 349.1339$, found $[\text{M}-\text{H}]^+ = 349.1321$.

4.7. General procedure for the synthesis of target compounds **SN46**

4.7.1. *N*-Hexyl-2-((6-methoxybenzo[d]thiazol-2-yl)amino)ethanethioamide (**SN46**)

The synthesis of the compounds was carried out by dissolving the compound **SN12** (1 mmol, 1.0 equiv) under 1,4-dioxane solvent (5 mL), adding Lawesson reagent (1.5 mmol, 1.5 equiv) with stirring, heating to 90 °C and reacting for 12 h to monitor the completeness of the reaction. Afterward, it was extracted with saturated NaHCO_3 solution and ethyl acetate and dried. Purification was carried out by rapid column chromatography with eluent ratio of 1:1 (PE:EA). The pure product was collected to give white solid **SN46** (193.0 mg, yield: 57.2%). ^1H NMR (400 MHz, $\text{DMSO-}d_6$) δ 8.20 (t, $J = 5.5$ Hz, 1H), 8.02 (s, 1H), 7.37–7.29 (m, 2H), 6.83 (dd, $J = 8.7, 2.7$ Hz, 1H), 4.58 (d, $J = 5.5$ Hz, 2H), 4.32 (t, $J = 7.0$ Hz, 2H), 3.74 (s, 3H), 1.77 (t, $J = 7.0$ Hz, 2H), 1.29–1.17 (m, 6H), 0.87–0.78 (m, 3H). ^{13}C NMR (101 MHz, $\text{DMSO-}d_6$) δ 164.72, 154.89, 146.91, 131.98, 123.42, 118.99,

113.42, 106.03, 56.01, 49.71, 39.36, 31.03, 30.18, 25.94, 22.38, 14.29. HRMS (ESI) of compound **SN46**: calcd for $C_{16}H_{23}N_3OS_2$ $[M-H]^+$ = 336.1209, found $[M-H]^+$ = 336.1202.

4.8. General procedure for the synthesis of target compounds **SN47** to **SN50**

4.8.1. 2-((6-Ethoxybenzo[d]thiazol-2-yl)amino)-N-hexylacetamide (**SN47**)

The compound was prepared with reference to compound **SN12** using 6-ethoxybenzo[d]thiazol-2-amine (1 mmol, 1.0 equiv) and hexylamine (1.2 mmol, 1.2 equiv) as raw material. The pure product was collected to give white solid **SN47** (141.0 mg, yield: 42.0%). 1H NMR (400 MHz, DMSO- d_6) δ 7.99 (dt, J = 24.7, 5.7 Hz, 2H), 7.34–7.20 (m, 2H), 6.80 (dd, J = 8.8, 2.6 Hz, 1H), 4.05–3.96 (m, 2H), 3.94 (t, J = 7.0 Hz, 2H), 3.07 (q, J = 6.6 Hz, 2H), 1.39 (t, J = 6.9 Hz, 3H), 1.31 (d, J = 7.1 Hz, 3H), 1.26–1.19 (m, 6H), 0.84 (q, J = 7.0 Hz, 3H). ^{13}C NMR (101 MHz, DMSO- d_6) δ 169.04, 165.08, 154.07, 146.69, 132.12, 118.89, 113.89, 106.67, 63.98, 47.12, 38.97, 31.46, 29.52, 26.47, 22.51, 15.22, 14.36. HRMS (ESI) of compound **SN47**: calcd for $C_{17}H_{25}N_3O_2S$ $[M-H]^+$ = 334.1594, found $[M-H]^+$ = 334.1586.

4.8.2. N-Hexyl-2-((6-hydroxybenzo[d]thiazol-2-yl)amino)acetamide (**SN48**)

The compound was prepared with reference to compound **SN12** using 2-aminobenzo[d]thiazol-6-ol (1 mmol, 1.0 equiv) and hexylamine (1.2 mmol, 1.2 equiv) as raw material. The pure product was collected to give white solid **SN48** (200.5 mg, yield: 65.2%). 1H NMR (400 MHz, DMSO- d_6) δ 9.13 (d, J = 1.4 Hz, 1H), 7.90 (dt, J = 11.0, 5.6 Hz, 2H), 7.17 (d, J = 8.5 Hz, 1H), 7.05 (d, J = 2.6 Hz, 1H), 6.66 (dd, J = 8.6, 2.5 Hz, 1H), 3.91 (d, J = 5.7 Hz, 2H), 3.07 (q, J = 6.5 Hz, 2H), 1.38 (d, J = 6.9 Hz, 2H), 1.27–1.21 (m, 6H), 0.88–0.80 (m, 3H). ^{13}C NMR (101 MHz, DMSO- d_6) δ 169.12, 164.30, 152.72, 145.59, 132.05, 118.93, 114.05, 107.40, 47.11, 39.73, 38.97, 31.46, 29.53, 26.47, 22.51, 14.37. HRMS (ESI) of compound **SN48**: calcd for $C_{15}H_{21}N_3O_2S$ $[M-H]^+$ = 306.1281, found $[M-H]^+$ = 306.1273.

4.8.3. N-Hexyl-2-((6-methylbenzo[d]thiazol-2-yl)amino)acetamide (**SN49**)

The compound was prepared with reference to compound **SN12** using 6-methylbenzo[d]thiazol-2-amine (1 mmol, 1.0 equiv) and hexylamine (1.2 mmol, 1.2 equiv) as raw material. The pure product was collected to give white solid **SN49** (195.7 mg, yield: 64.1%). 1H NMR (400 MHz, DMSO- d_6) δ 8.03 (d, J = 63.0 Hz, 2H), 7.46 (s, 1H), 7.25 (d, J = 8.1 Hz, 1H), 7.02 (d, J = 8.2 Hz, 1H), 3.95 (s, 2H), 3.07 (q, J = 6.6 Hz, 2H), 2.31 (s, 3H), 1.44–1.34 (m, 2H), 1.23 (s, 6H), 0.84 (t, J = 6.2 Hz, 3H). ^{13}C NMR (101 MHz, DMSO- d_6) δ 168.96, 165.97, 150.55, 131.20, 130.62, 126.94, 121.34, 118.23, 47.08, 38.98, 31.46, 29.52, 26.47, 22.51, 21.22, 14.37. HRMS (ESI) of compound **SN49**: calcd for $C_{16}H_{23}N_3OS$ $[M-H]^+$ = 304.1489, found $[M-H]^+$ = 304.1483.

4.8.4. N-Hexyl-2-((4-methoxybenzo[d]thiazol-2-yl)amino)acetamide (**SN50**)

The compound was prepared with reference to compound **SN12** using 4-methoxybenzo[d]thiazol-2-amine (1 mmol, 1.0 equiv) and hexylamine (1.2 mmol, 1.2 equiv) as raw material. The pure product was collected to give white solid **SN50** (160.5 mg, yield: 49.9%). 1H NMR (400 MHz, DMSO- d_6) δ 8.11 (q, J = 10.5, 8.1 Hz, 1H), 7.98 (d, J = 6.2 Hz, 1H), 7.26 (d, J = 8.0 Hz, 1H),

6.99 (t, J = 8.1 Hz, 1H), 6.84 (d, J = 7.8 Hz, 1H), 3.99 (d, J = 5.8 Hz, 2H), 3.83 (d, J = 7.4 Hz, 3H), 3.08 (q, J = 6.5 Hz, 2H), 1.39 (q, J = 7.1 Hz, 2H), 1.23 (s, 6H), 0.83 (d, J = 7.0 Hz, 3H). ^{13}C NMR (101 MHz, DMSO- d_6) δ 168.90, 165.41, 150.52, 141.89, 132.13, 122.23, 113.71, 108.50, 56.00, 47.09, 39.01, 31.46, 29.53, 26.49, 22.49, 14.37. HRMS (ESI) of compound **SN50**: calcd for $C_{16}H_{23}N_3O_2S$ $[M-H]^+$ = 320.1438, found $[M-H]^+$ = 320.1430.

4.9. Bacterial strains and cells

P. aeruginosa PAO1, PAO1- Δ lasI Δ rhII, PAO1-*gfp*, PAO1-*lasB-gfp*, PAO1-*gacS-gfp*, PAO1-*gacA-gfp*, PAO1-*rsmY-gfp*, PAO1-*rsmZ-gfp*, Δ rsmY, Δ rsmZ, Δ gacA and the clinical *P. aeruginosa* strains (PA3137, PA1313) were used. Store bacteria in LB broth supplemented with 25% (v/v) glycerol at $-80^\circ C$. Before each experiment, incubate the inoculum from frozen original seeds on LB agar plates overnight at $37^\circ C$ to obtain a single colony. Single colonies were selected and placed in LB broth. They were cultured overnight at $37^\circ C$ and 200 rpm, and diluted to the required concentration according to the optical density at 600 nm.

4.10. Biofilm formation analysis

P. aeruginosa PAO1 was diluted with ABTGC (B-medium (0.1% $MgCl_2$, 0.1% $CaCl_2$, 0.1% $FeCl_3$) supplemented with 10% A10, 0.2% glucose, and 0.2% casamino acids) medium at OD₆₀₀ of 0.02 and added to a 96-well plate with 75 μ L of bacterial culture containing **SN12** and 75 μ L of already diluted bacteria in each well. Equal volume of ABTGC medium was added as control. Inoculated plates were incubated under static conditions at $37^\circ C$ for 24 h. Planktonic cells were removed, and the biofilms were rinsed with PBS. Biofilms were stained by 150 μ L of 0.1% crystal violet for 15 min, followed by rinsing with distilled water. The cell-associated dye was solubilized in 150 μ L of 30% acetic acids in water and optical density (OD) of each well was measured at 570 nm using a microplate reader (Bio Tek, USA).

4.11. MIC assay

P. aeruginosa PAO1 was grown overnight in MH broth and diluted at a final bacterial concentration achieving an OD₆₀₀ of 0.05 in 96-well plates. Then, 100 μ L of culture medium containing different concentrations of **SN12** were added to the plates. After incubating for 20 h at $37^\circ C$, the absorbance values of each well were measured at 600 nm by a microplate reader (Bio Tek, USA).

4.12. Cytotoxicity assay

The cytotoxicity assay of the compounds was performed by MTT method. LO2, A549, DLD-1 cell seed plates were incubated in 96-well plates at a cell density of 0.6×10^3 cells/well for 24 h. The cells were treated with different concentrations (0, 1.25, 2.5, 5, 10, 25, 50, 100, and 200 μ mol/L) of compounds. After 24 h of treatment, 20 μ L MTT solution (5 mg/mL) was added to each well. After incubation for 4 h at $37^\circ C$, the absorbance was immediately measured at 570 nm using a microplate reader⁶⁰.

4.13. Zebrafish toxicity assay

The zebrafish toxicity assay of the compounds was performed by soaking method. 3–4 days zebrafish embryos of normal

development were selected and cultured in PTU embryo culture medium, which contained different concentrations (0, 25, 50, 100 and 200 $\mu\text{mol/L}$) of compound **SN12**, 10 strips/well. The survival rate was recorded at different times⁶¹.

4.14. Hemolysis assay

4% mouse or rabbit red blood cells (RBC) were washed in PBS and diluted to a concentration of 2%. Compound **SN12** was added individually to 100 μL of 2% RBC at a concentration of 0, 0.3125, 0.625, 1.25, 2.5, 5 and 10 $\mu\text{mol/L}$ in a 1.5 mL centrifuge tube. PBS alone and 0.4% Triton X-100 were used for negative control and positive control (100% hemolysis), respectively. Each reaction was repeated in triplicate. Plates were incubated for 2 h at 37 °C. Following incubation, samples were centrifuged at 2500 r for 5 min, and 100 μL of supernatant was transferred to a 96-well plate. Percent hemolysis for each sample was determined at 575 nm. The hemolysis rate was calculated according to Eq. (1)⁶²:

$$\text{Hemolysis (\%)} = (\text{OD}_{\text{sample}} - \text{OD}_{\text{negative}}) / (\text{OD}_{\text{positive}} - \text{OD}_{\text{negative}}) \times 100 \quad (1)$$

4.15. RT-PCR assay

Total RNA from the PAO1 was extracted using the Hipure Universal RNA kit (Magen, Shanghai, China) according to the manufacturer's protocol. The RNA concentration was detected by a NanoDrop2000 ultra-micro spectrophotometer. Then RNA was reverse transcribed using Hieff[®] qPCR SYBR Green Master Mix (No Rox). PCR was performed with the LightCycler[®] 480 Instrument II (Roche, Switzerland). Specific primers are listed in [Supporting Information Table S1](#). Rpsl was used as an internal control. All samples were analyzed in triplicate.

4.16. Ethics statement

All animal experiments were performed with approval from the Experimental Animal Ethics Committee of Jinan University. And the experiment was performed in accordance with National Regulations on Animal Experimentation (GB/T 35892-2018).

4.17. The wound infection model in mice

A murine wound infection model in BALB/c mice was established as previously described¹⁸. Three to five weeks healthy female mice ($n = 5$) were provided by SPF (Beijing) biotechnology Co., Ltd. Compound **SN12** was dissolved in saline containing 0.1% Tween 80 and antibiotics were prepared in saline. First, mice were anesthetized and then shaved on the back. A ~ 5 mm wound was created on the back of the mice and then 30 μL of *P. aeruginosa* PAO1 (5×10^8 CFU) was inoculated on the surface of the wound. Surrounded by 24 h of wound infection, the wound was treated with saline, antibiotics alone, or antibiotics in combination with compound **SN12**, respectively. The drugs were administered once a day. Then, a homogenate of the skin at the wound site was prepared and the CFU counting was obtained on an agar plate. Meanwhile, the wounds and body weights of the mice were monitored daily. After 9 days, the mice were euthanized and the

hearts, livers, spleens, lungs, and kidneys were taken for H&E analysis.

4.18. Bacterial growth curves analysis

Overnight cultures *P. aeruginosa* PAO1 were grown in LB medium at 37 °C and diluted with ABTGC to an initial OD₆₀₀ of 0.02. 75 μL of bacterial culture containing **SN12** and 75 μL of already diluted bacteria were added to a 96-well plate. The density of the cell suspensions was detected at 600 nm at 10-min intervals for 24 h at 37 °C.

4.19. Confocal laser scanning microscopy assays

P. aeruginosa PAO1 was inoculated with compounds **SN12** in a glass-bottom 96-well plate at 37 °C for 24 h. Then supernatant was removed, and the well surface was rinsed briefly with PBS three times. 100 μL of PBS containing 1 $\mu\text{mol/L}$ of SYTO9 and 10 $\mu\text{mol/L}$ of PI dye were added into the well¹⁹. The plate was incubated for 15 min in the dark. The effect of **SN12** on bacterial biofilm formation was observed by fluorescence confocal microscopy (Zeiss LSM800).

4.20. GFP reporter strain assays

The overnight culture of PAO1-*gfp* and PAO1-*lasB-gfp* was diluted in ABTGC medium containing different concentrations of compounds **SN12**. GFP fluorescence (excitation wavelength is 485 nm, emission wavelength is 528 nm) and OD₆₀₀ were measured by Bio Tek every 15 min at 37 °C for at least 16 h. For PAO1-*gacS-gfp*, PAO1-*gacA-gfp*, PAO1-*rsmY-gfp*, PAO1-*rsmZ-gfp*, Modified Mg²⁺ free M9 medium (6.78 g/L Na₂HPO₄, 3 g/L KH₂PO₄, 0.5 g/L NaCl₂, 1 g/L NH₄SO₄, 100 $\mu\text{mol/L}$ CaCl₂, 0.4% glucose) medium was used to instead of ABTGC, and GFP fluorescence was measured every 2 h.

4.21. Elastase assay

An overnight culture of *P. aeruginosa* PAO1 and PAO1-*ΔlasIΔrhII* in LB medium was diluted in 5 mL of ABTGC medium to a final optical density at 600 nm of 0.01. The culture was incubated with different concentrations of compounds **SN12** for 20 h at 37 °C, 200 rpm. The supernatant was collected after centrifugation at 10,000 rpm for 10 min and filtered by 0.2 $\mu\text{mol/L}$ filter. Elastase activity was measured with an EnzChekElastase assay kit (Invitrogen, USA). Fluorescence signals (excitation wavelength of 490 nm and emission wavelength of 520 nm) were recorded every 10 min at 37 °C for at least 4 h⁶³.

4.22. Motility assay

For swarming motility, petri dish was filled with 20 mL of LB medium supplemented with 0.5% (w/v) Bacto agar (Becton, Dickinson and Co.) and 0.5% (w/v) glucose in the presence of **SN12** and dried for 1 h at room temperature⁴⁴. Then a 1 μL drop of *P. aeruginosa* PAO1 was inoculated onto the surface of the Petri dish. For swimming motility, petri dish was filled with 20 mL of LB medium supplemented with 0.3% (w/v) Bacto agar and 0.5% (w/v) glucose in the presence of **SN12** and dried for 1 h at room temperature. Then a 1 μL drop of *P. aeruginosa* PAO1 was

inoculated into the middle of the Petri dish. The Petri dishes were incubated for 16 h at 37 °C.

4.23. Extracellular polysaccharides assay

P. aeruginosa PAO1 was respectively cocultured with equal volumes of **SN12** with different concentrations for 24 h, and ABTGC as a control. The biofilms were washed with 200 µL of saline and centrifuged for 10 min (4 °C, 10,000 rpm). Extracellular polysaccharide was extracted with 500 µL of 1.0 mol/L sodium hydroxide at 37 °C and centrifuged again. The supernatant was heated with 6% phenol and concentrated sulfuric acid for 30 min. The solution was cooled to room temperature and the OD₄₉₀ was measured.

4.24. Bacterial resistance development studies

P. aeruginosa PAO1 and the clinical strains of *P. aeruginosa* (PA1313, PA3137) were diluted in 2 mL of MH broth containing antibiotic Cip and Tob with or without **SN12**. Incubated the bacterial for 20 h at 37 °C, 200 rpm. Then, the absorbance of the bacteria at 600 nm was measured using a microplate reader (Bio Tek, USA). Bacterial suspension from sub-MIC (0.5 × MIC) of antibiotics or combination of antibiotics and **SN12** was used to prepare the inoculum for the next day MIC experiment. The ratio of the MIC obtained during each day relative to the MIC at 0 day (first time exposure) was determined. The data were expressed as increase in MIC of antibiotic with each passage⁶⁴.

4.25. Tandem mass tag (TMT) proteomics analysis

An overnight culture of *P. aeruginosa* PAO1 in LB medium was diluted in 5 mL of ABTGC medium to a final optical density at 600 nm of 0.01. The culture was incubated with 1 µmol/L of **SN12** for 24 h at 37 °C, 200 rpm. The bacterial cells were obtained after centrifugation at 4000 rpm for 10 min and washed three times with PBS. The protein extraction and testing were completed by Fitgene Biotech Co., Ltd. This was done as follows, bacteria were lysed using lysis solution L3 (with SDS) (Fitgene Biotech Co., item no. FP1803) and proteins were precipitated using acetone. A standard curve was made using fetal bovine serum standard BSA (concentration of 5 µg/µL) (Sigma, Article No.: C503061-1250), and 20 µL of the sample was taken out and then stained with Bradford's staining solution (595 nm) (Fitgene Biotech Co., Article No.: FP1806) to quantify the proteins. After quantification, proteins were subjected to protein FASP digestion, mainly using trypsin (Promega, Article No. V5280). A 100 µL sample (100 µg of digested product) was taken and labeled using a TMT kit (Thermo, Article No.: A44522). After labeling, the samples were first subjected to a first-dimensional high pH-RP liquid phase separation using a liquid chromatograph LC-20AD (one-dimensional) (Shimadzu). This was followed by a two-dimensional reversed-phase RPLC-MS separation using a liquid chromatograph Dionex Ultimate 3000 RSLCnano (two-dimensional) (Thermo Scientific). The separated peptides were then fed directly into a mass spectrometer Thermo Scientific Q Exactive for online detection.

4.26. Ensemble docking and RMSD simulations

Apo protein (PDB ID: 5O7J) was prepared in Maestro protein preparation tool⁴¹. An orthorhombic solvent box filled with SPC

water molecules, counter ions and additional 0.15 mol/L concentration of NaCl was constructed in Desmond system builder⁴¹. A 200ns molecular dynamics was first performed after standard energy minimization and equilibrium whole system to sample the protein conformation space. Trajectory was clustered based on RMSD matrix of backbone atoms. All representative structures were scanned by SiteMap to search potential binding sites⁴⁰. Potential sites obtained were first screened by criteria of sitescore (>0.8) and volume (>150), top ones were then visually inspected. Site 22 with preferable score and size on all conformation clusters were proceed into docking with **SN12**³⁹. Top 5 binding complexes based on docking score were further validated in additional 100 ns MD simulation, regular protein–ligand job settings were applied³⁷, and protein–ligand interactions were analyzed with interaction diagram tool, the binding free energy was calculated based on equilibrium trajectory via MM-GBSA method⁶⁵.

4.27. SEM assays

Overnight cultured *P. aeruginosa* PAO1 was diluted with LB medium to an OD₆₀₀ of 0.05 and then incubated for 16 h with different concentrations of **SN12** (0, 0.625, 0.125, 0.25, 0.5 and 40 µmol/L). The precipitates were then eluted with gradients of 30%, 50%, 70%, 90% and 100% ethanol. Finally, these samples were placed on silicon wafers for SEM¹⁸.

4.28. Statistical analysis

Data are presented as mean ± SD. One-way analysis of variance (ANOVA) was used for multiple-group comparison. Intergroup comparison was analyzed by Tukey's multiple comparison test. **P* ≤ 0.05, ***P* ≤ 0.01, ****P* ≤ 0.001 and *****P* ≤ 0.0001.

4.29. Construction of plasmid

DNA cloning and plasmid preparation were performed according to standard methods. PCR primers were designed with restriction sites at their ends for subsequent digestion and ligation into the specific vector (Supporting Information Table S1). For constructing pET-28a-GacS (residues 12–166), the primer pair GacSf and GacSr was used to amplify the GacS (residues 12–166) fragment from the genomic DNA. Vector was digested with BamHI and HindIII restriction enzymes and purified. The PCR products were digested and inserted into pET-28a to generate pET-28a-GacS (residues 12–166) using the Seamless cloning kit. The resulting plasmid was transformed into *E. coli* DH5α, and the plasmid construct was verified by sequencing using primers that annealed to sites outside the multiple cloning site.

4.30. Protein expression and purification

The plasmid pET-28a-GacS (residues 12–166) was transformed into *E. coli* BL21 (DE3) in which the GacS (residues 12–166) protein was expressed contains a 6-His tag. GacS (residues 12–166) was induced by 0.5 mmol/L IPTG for overnight at 16 °C. Cells were harvested and resuspended in binding buffer (30 mmol/L HEPES pH 7.5, 150 mmol/L NaCl, and 10 mmol/L imidazole). Bacteria were lysed using probe sonication for 40 min, and cell debris were removed by centrifugation at 15,000 rpm for 30 min. The supernatant was loaded to a Ni-NTA column (L00250-50, GeneScript).

4.31. Microscale thermophoresis (MST)

The GacS (12–166)-His protein, at a 100 nmol/L concentration, was subjected to fluorescent tagging using a His-tag labeling kit (Nano Temper, MO-L008), adhering to the guidelines specified in the user manual. After the labeling was finalized, 10 μ L of the fluorescently tagged GacS (12–166)-His protein was mixed with 10 μ L of PBST buffer, followed by the addition of SN12 at a concentration of 1 mmol/L. This mixture was then subject to serial dilution. The microscale thermophoresis assay was carried out on a NanoTemper Monolith NT.115 device, set to 100% LED power and medium MST power setting. Data collected from the assay were analyzed using the MO. Affinity Analysis software (X86).

Acknowledgments

This work was supported by the National Natural Science Foundation of China (No. 22177039 and 82304274), National Key R&D Program of China (No. 2021YFC2300400), China Postdoctoral Science Foundation (No. 55350658). We thank Dr Liang Yang from the School of Medicine, Southern University of Science and Technology for the donation of PAO1-*gfp*, PAO1-*gacA-gfp*, PAO1-*gacS-gfp* and PAO1-*rsmZ-gfp*, PAO1-*rsmY-gfp* strains and the First Affiliated Hospital of Jinan University Clinical Laboratory for the donation of four multidrug-resistant (MDR) strains. We thank Dr Lian Hui Zhang from Integrative Microbiology Research Center, South China Agricultural University for the donation of Δ gacA, Δ rsmY, and Δ rsmZ strains.

Author contributions

Pinghua Sun, Junxia Zheng, and Haibo Zhou designed and supervised the experiments and revised the manuscript. Kaihe Ye, Jianfu Zhao, Jun Xu, and Meiyang Huang provided critical reading and revision of the manuscript. Jun Liu, Wenfu Wu, and Jiayi Hu wrote the manuscript, performed biological assessments experiments and analyzed the data. Siyu Zhao, Qiuxian Chen, Yujie Li, Jie Tang, and Xiao Wu performed some biological assessments experiments. Jun Liu, Wenfu Wu, and Jiayi Hu performed synthesis experiments. Yiqun Chang performed silico study. Qiang Zhang, Zhenmeng Zhang, Jiarui Du, Shumeng Jiao, and Haichuan Xiao performed some synthesis experiments. All authors have approved the final version of the manuscript.

Conflicts of interest

Pinghua Sun, Jun Liu, Wenfu Wu, and Jiayi Hu (inventors) declare that they have filed a Chinese patent application (CN116554124A) based on the findings in this paper. The authors declare no competing interests.

Appendix A. Supporting information

Supporting information to this article can be found online at <https://doi.org/10.1016/j.apsb.2024.08.002>.

References

- MacLean RC, Millan AS. The evolution of antibiotic resistance. *Science* 2019;**365**:1082–3.
- Larsson DJ, Flach CF. Antibiotic resistance in the environment. *Nat Rev Microbiol* 2022;**20**:257–69.
- Zhao XL, Chen ZG, Yang TC, Jiang M, Wang J, Cheng ZX, et al. Glutamine promotes antibiotic uptake to kill multidrug-resistant uropathogenic bacteria. *Sci Transl Med* 2021;**13**:eabj0716.
- Nadar S, Khan T, Patching SG, Omri A. Development of antibiofilm therapeutics strategies to overcome antimicrobial drug resistance. *Microorganisms* 2022;**10**:303–28.
- Butler MS, Gigante V, Sati H, Paulin S, Al-Sulaiman L, Rex JH, et al. Analysis of the clinical pipeline of treatments for drug-resistant bacterial infections: despite progress, more action is needed. *Antimicrob Agents Chemother* 2022;**66**:e01991–21.
- Antimicrobial Resistance Collaborators. Global burden of bacterial antimicrobial resistance in 2019: a systematic analysis. *Lancet* 2022;**399**:629–55.
- Reynolds D, Kollef M. The epidemiology and pathogenesis and treatment of *Pseudomonas aeruginosa* infections: an update. *Drugs* 2021;**81**:2117–31.
- Fleming D, Rumbaugh KP. Approaches to dispersing medical biofilms. *Microorganisms* 2017;**5**:15–6.
- Ram RJ, VerBerkmoes NC, Thelen MP, Tyson GW, Baker BJ, Blake RC, et al. Community proteomics of a natural microbial biofilm. *Science* 2005;**308**:1915–20.
- Cendra MDM, Torrents E. *Pseudomonas aeruginosa* biofilms and their partners in crime. *Biotechnol Adv* 2021;**49**:107734–15.
- Hoyle BD, Costerton WJ. Bacterial resistance to antibiotics: the role of biofilms. *Prog Drug Res* 1991;**37**:91–105.
- Trubenová B, Roizman D, Moter A, Rolff J, Regoes RR. Population genetics, biofilm recalcitrance, and antibiotic resistance evolution. *Trends Microbiol* 2022;**30**:841–52.
- Kolpen M, Kragh KN, Enciso JB, Faurholt-Jepsen D, Lindegaard B, Egelund GB, et al. Bacterial biofilms predominate in both acute and chronic human lung infections. *Thorax* 2022;**77**:1015–22.
- Mah TFC, O'Toole GA. Mechanisms of biofilm resistance to antimicrobial agents. *Trends Microbiol* 2001;**9**:34–9.
- Lin L, Chi J, Yan Y, Luo R, Feng X, Zheng Y, et al. Membrane-disruptive peptides/peptidomimetics-based therapeutics: promising systems to combat bacteria and cancer in the drug-resistant era. *Acta Pharm Sin B* 2021;**11**:2609–44.
- Cappiello F, Loffredo MR, DelPlato C, Cammarone S, Casciaro B, Quaglio D, et al. The reevaluation of plant-derived terpenes to fight antibiotic-resistant infections. *Antibiotics* 2020;**9**:325–34.
- Abouelhasan Y, Garrison AT, Yang H, Chávez-Riveros A, Burch GM, Huigens IIRW. Recent progress in natural-product-inspired programs aimed to address antibiotic resistance and tolerance. *J Med Chem* 2019;**62**:7618–42.
- Liu J, Zhao SY, Hu JY, Chen QX, Jiao SM, Xiao HC, et al. Novel coumarin derivatives inhibit the quorum sensing system and iron homeostasis as antibacterial synergists against *Pseudomonas aeruginosa*. *J Med Chem* 2023;**66**:14735–54.
- Liu J, Hou JS, Li YB, Miao ZY, Sun PH, Lin J, et al. Novel 2-substituted 3-hydroxy-1,6-dimethylpyridin-4(1H)-ones as dual-acting biofilm inhibitors of *Pseudomonas aeruginosa*. *J Med Chem* 2020;**63**:10921–45.
- Goswami M, Espinasse A, Carlson EE. Disarming the virulence arsenal of *Pseudomonas aeruginosa* by blocking two-component system signaling. *Chem Sci* 2018;**9**:7332–7.
- Xia FW, Guo BW, Zhao Y, Wang JL, Chen Y, Pan X, et al. Type I photosensitizer targeting glycans: overcoming biofilm resistance by inhibiting the two-component system, quorum sensing, and multidrug efflux. *Adv Mater* 2023;**35**:2309797–18.
- Francis VI, Waters EM, Finton-James SE, Gori A, Kadioglu A, Brown AR, et al. Multiple communication mechanisms between sensor kinases are crucial for virulence in *Pseudomonas aeruginosa*. *Nat Commun* 2018;**9**:2219–11.
- Trouillon J, Imbert L, Villard AM, Vernet T, Attrée I, Elsen S. Determination of the two-component systems regulatory network

- reveals core and accessory regulations across *Pseudomonas aeruginosa* lineages. *Nucleic Acids Res* 2021;**49**:11476–90.
24. Bhagirath AY, Li Y, Patidar R, Yerex K, Ma X, Kumar A, et al. Two component regulatory systems and antibiotic resistance in gram-negative pathogens. *Int J Mol Sci* 2019;**20**:1781–30.
 25. Skerker JM, Prasol MS, Perchuk BS, Biondi EG, Laub MT. Two-component signal transduction pathways regulating growth and cell cycle progression in a bacterium: a system-level analysis. *PLoS Biol* 2005;**3**:e334–19.
 26. Brencic A, McFarland KA, McManus HR, Castang S, Mogno I, Dove SL, et al. The GacS/GacA signal transduction system of *Pseudomonas aeruginosa* acts exclusively through its control over the transcription of the RsmY and RsmZ regulatory small RNAs. *Mol Microbiol* 2009;**73**:434–45.
 27. Xuan G, Lin H, Li X, Kong J, Wang J. RetS regulates phage infection in *Pseudomonas aeruginosa* via modulating the GacS/GacA two-component system. *J Virol* 2022;**96**:e00197–22.
 28. Broder UN, Jaeger T, Jenal U. LadS is a calcium-responsive kinase that induces acute-to-chronic virulence switch in *Pseudomonas aeruginosa*. *Nat Microbiol* 2016;**2**:1–11.
 29. Wei X, Huang X, Tang L, Wu D, Xu Y. Global control of GacA in secondary metabolism, primary metabolism, secretion systems, and motility in the rhizobacterium *Pseudomonas aeruginosa* M18. *J Bacteriol* 2013;**195**:3387–400.
 30. Liu J, Hou JS, Chang YQ, Peng LJ, Zhang XY, Miao ZY, et al. New pqs quorum sensing system inhibitor as an antibacterial synergist against multidrug-resistant *Pseudomonas aeruginosa*. *J Med Chem* 2022;**65**:688–709.
 31. Liu J, Meng Y, Yang MH, Zhang XY, Zhao JF, Sun PH, et al. Design, synthesis and biological evaluation of novel 3-hydroxypyridin-4(1H)-ones based hybrids as *Pseudomonas aeruginosa* biofilm inhibitors. *Eur J Med Chem* 2023;**259**:115665–18.
 32. Wilke KE, Francis S, Carlson EE. Inactivation of multiple bacterial histidine kinases by targeting the ATP-binding domain. *ACS Chem Biol* 2015;**10**:328–35.
 33. Borriello G, Werner E, Roe F, Kim AM, Ehrlich GD, Stewart PS. Oxygen limitation contributes to antibiotic tolerance of *Pseudomonas aeruginosa* in biofilms. *Antimicrob Agents Chemother* 2004;**48**:2659–64.
 34. Costa KC, Glasser NR, Conway SJ, Newman DK. Pyocyanin degradation by a tautomerizing demethylase inhibits *Pseudomonas aeruginosa* biofilms. *Science* 2017;**355**:170–3.
 35. Qin S, Xiao W, Zhou C, Pu Q, Deng X, Lan L, et al. *Pseudomonas aeruginosa*: pathogenesis, virulence factors, antibiotic resistance, interaction with host, technology advances and emerging therapeutics. *Signal Transduction Targeted Ther* 2022;**7**:199–27.
 36. Goodman AL, Merighi M, Hyodo M, Ventre I, Filloux A, Lory S. Direct interaction between sensor kinase proteins mediates acute and chronic disease phenotypes in a bacterial pathogen. *Genes Dev* 2009;**23**:249–59.
 37. Ali-Ahmad A, Fadel F, Sebban-Kreuzer C, Ba M, Pélissier GD, Bornet O, et al. Structural and functional insights into the periplasmic detector domain of the GacS histidine kinase controlling biofilm formation in *Pseudomonas aeruginosa*. *Sci Rep* 2017;**7**:11262–13.
 38. Amaro RE, Baudry J, Chodera J, Demir Ö, McCammon JA, Miao Y, et al. Ensemble docking in drug discovery. *Biophys J* 2018;**114**:2271–8.
 39. *Schrödinger Release 2023-1: SiteMap*. New York, NY: Schrödinger, LLC; 2023.
 40. *Schrödinger release 2023-1: glide*. New York, NY: Schrödinger, LLC; 2023.
 41. *Schrödinger Release 2023-1: Desmond molecular dynamics dystem*. New York, NY: D. E. Shaw Research; 2023.
 42. Kaler KMR, Nix JC, Schubot FD. RetS inhibits *Pseudomonas aeruginosa* biofilm formation by disrupting the canonical histidine kinase dimerization interface of GacS. *J Biol Chem* 2021;**297**:101193–13.
 43. Kay E, Humair B, Déneraud V, Riedel K, Spahr S, Eberl L, et al. Two GacA-dependent small RNAs modulate the quorum-sensing response in *Pseudomonas aeruginosa*. *J Bacteriol* 2006;**188**:6026–33.
 44. Lee J, Zhang L. The hierarchy quorum sensing network in *Pseudomonas aeruginosa*. *Protein Cell* 2015;**6**:26–41.
 45. Liu J, Chen QX, Wu WF, Wang D, Zhao SY, Li JH, et al. Novel ligustilide derivatives target quorum sensing system LasR/LasB and relieve inflammatory response against *Pseudomonas aeruginosa* infection. *Eur J Med Chem* 2024;**263**:115972–19.
 46. Grace A, Sahu R, Owen DR, Dennis VA. *Pseudomonas aeruginosa* reference strains PAO1 and PA14: a genomic, phenotypic, and therapeutic review. *Front Microbiol* 2022;**13**:1023523–15.
 47. Verstraeten N, Braeken K, Debkumari B, Fauvart M, Fransaeer J, Vermant J, et al. Living on a surface: swarming and biofilm formation. *Trends Microbiol* 2008;**16**:496–506.
 48. Grobas I, Polin M, Asally M. Swarming bacteria undergo localized dynamic phase transition to form stress-induced biofilms. *Elife* 2021;**10**:e62632–22.
 49. Gooderham WJ, Hancock REW. Regulation of virulence and antibiotic resistance by two-component regulatory systems in *Pseudomonas aeruginosa*. *FEMS Microbiol Rev* 2009;**33**:279–94.
 50. O'Toole GA, Kolter R. Flagellar and twitching motility are necessary for *Pseudomonas aeruginosa* biofilm development. *Mol Microbiol* 1998;**30**:295–304.
 51. Rashid MH, Kornberg A. Inorganic polyphosphate is needed for swimming, swarming, and twitching motilities of *Pseudomonas aeruginosa*. *Proc Natl Acad Sci U S A* 2000;**97**:85–90.
 52. Simner PJ, Mostafa HH, Bergman Y, Ante M, Tekle T, Adebayo A, et al. Progressive development of cefiderocol resistance in *Escherichia coli* during therapy is associated with an increase in bla_{NDM-5} copy number and gene expression. *Clin Infect Dis* 2022;**75**:47–54.
 53. Göttig S, Frank D, Mungo E, Nolte A, Hogardt M, Besier S, et al. Emergence of ceftazidime/avibactam resistance in KPC-3-producing *Klebsiella pneumoniae* in vivo. *J Antimicrob Chemother* 2019;**74**:3211–6.
 54. Hewer SCL, Smith S, Rowbotham NJ, Yule A, Smyth AR. Antibiotic strategies for eradicating *Pseudomonas aeruginosa* in people with cystic fibrosis. *Cochrane Database Syst Rev* 2023;**4**:CD004197–5.
 55. Pelegrin AC, Palmieri M, Mirande C, Oliver A, Moons P, Goossens H, et al. *Pseudomonas aeruginosa*: a clinical and genomics update. *FEMS Microbiol Rev* 2021;**45**:fuab026–20.
 56. Finbloom JA, Raghavan P, Kwon M, Kharbikar BN, Yu MA, Desai TA. Codelivery of synergistic antimicrobials with polyelectrolyte nanocomplexes to treat bacterial biofilms and lung infections. *Sci Adv* 2023;**9**:eade8039–11.
 57. Lei E, Tao H, Jiao S, Yang A, Zhou Y, Wang M, et al. Potentiation of vancomycin: creating cooperative membrane lysis through a “derivatization-for-sensitization” approach. *J Am Chem Soc* 2022;**144**:10622–39.
 58. Derek KKC, Katherine D, Mahrukh F, Hanjeong H, Ikram Q, Lori L. Burrows nutrient limitation sensitizes *Pseudomonas aeruginosa* to vancomycin. *ACS Infect Dis* 2023;**9**:1408–23.
 59. Yan DY, Huang Y, Zhang JY, Wu Q, Song GJ, Ji J, et al. Adding flying wings: butterfly-shaped NIR-II AIEgens with multiple molecular rotors for photothermal combating of bacterial biofilms. *J Am Chem Soc* 2023;**145**:25705–15.
 60. Kamiloglu S, Sari G, Ozdal T, Capanoglu E. Guidelines for cell viability assays. *Food Front* 2020;**1**:332–49.
 61. Merino C, Casado M, Piña B, Vinaixa M, Ramírez N. Toxicity of 4-(methylnitrosamino)-1-(3-pyridyl)-1-butanone (NNK) in early development: a wide-scope metabolomics assay in zebrafish embryos. *J Hazard Mater* 2022;**429**:127746–8.
 62. Zou HX, Koh JJ, Li JG, Qiu SX, Aung TT, Lin HF, et al. Design and synthesis of amphiphilic xanthone-based, membrane-targeting antimicrobials with improved membrane selectivity. *J Med Chem* 2013;**56**:2359–73.

63. Furiga A, Lajoie B, El Hage S, Baziard G, Roques C. Impairment of *Pseudomonas aeruginosa* biofilm resistance to antibiotics by combining the drugs with a new quorum-sensing inhibitor. *Antimicrob Agents Chemother* 2016;**60**:1676–86.
64. Tan SY, Chua S, Chen Y, Rice SA, Kjelleberg S, Nielsen TE, et al. Identification of five structurally unrelated quorum-sensing inhibitors of *Pseudomonas aeruginosa* from a natural-derivative database. *Antimicrob Agents Chemother* 2013;**57**:5629–41.
65. Wang E, Sun H, Wang J, Wang Z, Liu H, Zhang JZ, et al. End-point binding free energy calculation with MM/PBSA and MM/GBSA: strategies and applications in drug design. *Chem Rev* 2019;**119**:9478–508.